Vangl2-dependent regulation of membrane protrusions and directed migration requires a fibronectin extracellular matrix

Anna M. Love, Dianna J. Prince, and Jason R. Jessen*

Department of Biology, Middle Tennessee State University, Murfreesboro, TN, USA.

*Corresponding author: Jason R. Jessen
telephone: (615) 898-2060
email: jason.jessen@mtsu.edu
address: Middle Tennessee State University
Department of Biology
P.O. Box 60
Murfreesboro, TN 37132

Key words:
Vangl2, fibronectin, protrusion, polarity, migration, gastrulation

ABSTRACT

During zebrafish gastrulation the planar cell polarity (PCP) protein Vang-like 2 (Vangl2) regulates polarization of cells engaged in directed migration. However, it is unclear whether Vangl2 influences membrane-protrusive activities in migrating gastrula cells and if these processes require the fibronectin extracellular matrix. We report that Vangl2 modulates formation and polarization of actin-rich filopodia-like and large lamellipodia-like protrusions in ectodermal cells. By contrast, disrupted Glypican4/PCP signaling affects protrusion polarity but not protrusion number or directed migration. Analysis of fluorescent fusion protein expression suggests widespread Vangl2 symmetry in migrating cells but enrichment at membrane domains with developing large protrusions compared to non-protrusive domains. We show the fibronectin extracellular matrix is essential for cell surface Vangl2 expression, membrane-protrusive activity, and directed migration. Manipulation of fibronectin protein levels rescues protrusion and directed migration phenotypes in *vangl2* mutant embryos, but is not sufficient to restore PCP and convergence and extension movements. Together, our findings identify distinct roles for Vangl2 and Glypican4/PCP signaling during membrane protrusion formation and demonstrate cell-matrix interactions underlie Vangl2-dependent regulation of protrusive activities in migrating gastrula cells.

SUMMARY STATEMENT

This paper examines planar cell polarity protein function during membrane protrusion formation and polarization in migrating gastrula cells and demonstrates a requirement for the extracellular matrix protein fibronectin.

INTRODUCTION

Establishment of planar cell polarity (PCP) is a complex process involving many proteins functioning cell autonomously and/or non-autonomously. First described in reference to the orientation of insect hairs and bristles (Lawrence, 1966; Nubler-Jung et al., 1987), PCP and its associated proteins are linked to a variety of morphogenetic processes, including gastrulation movements (Goodrich and Strutt, 2011; Gray et al., 2011; Jessen and Solnica-Krezel, 2005). The six core PCP genes identified in fly include *van gogh*, *prickle*, *dishevelled*, *frizzled*, *flamingo*, and *diego* (Strutt and Strutt, 2007; Wong and Adler, 1993; Wu and Mlodzik, 2009). Genetic evidence that a core PCP protein is required for vertebrate gastrulation came with identification of the four-pass transmembrane protein *vang-like 2* (*vangl2*) as the defective gene in *trilobite* mutant zebrafish (*Danio rerio*) embryos (Jessen et al., 2002; Solnica-Krezel et al., 1996). Loss of Vangl2 produces a strong convergence and extension gastrulation phenotype, characterized by shortened and broadened embryonic body axes. Underlying convergence and extension are several cell behaviors, among them directed migration and mediolateral intercalation. Here, PCP is defined as the elongation and mediolateral alignment (MLA) of ectodermal and mesodermal cells perpendicular to the dorsal embryonic axis. Loss of Vangl2 causes lateral cells to meander, moving dorsally along indirect trajectories (Jessen et al., 2002). How Vangl2 regulates directed migration during zebrafish gastrulation is not understood.

Accumulating data show a non-canonical Wnt pathway controls PCP during gastrulation. With the aid of the glycosylphosphatidylinositol-anchored Glypican4 co-receptor, Wnt11 and Wnt5b bind Frizzled receptors to effect changes in the subcellular distribution of Dishevelled (Heisenberg et al., 2000; Kilian et al., 2003; Ohkawara et al., 2003; Topczewski et al., 2001). Downstream, Rho family small GTPases and their effector proteins (e.g. Rho kinase) are thought to stimulate changes in actin arrangement and cell polarization (Habas et al., 2003; Habas et al., 2001; Marlow et al., 2002). Vangl2 and its cytoplasmic binding partner, Prickle1a, somehow influence the Glypican4/PCP pathway (Carreira-Barbosa et al., 2003; Dohn et al., 2013; Jessen et al., 2002; Veeman et al., 2003), perhaps by regulating Dishevelled signaling (Seo et al., 2017). Zebrafish with null mutations in *vangl2* and *glypican4*/*knypek* or *vangl2* and *wnt11*/*silberblick* have convergence and extension phenotypes stronger than the individual mutants (Heisenberg and Nusslein-Volhard, 1997; Marlow et al., 1998). These findings indicate Vangl2 and Glypican4 have distinct functions during gastrulation movements

A hallmark of PCP in fly epithelium is asymmetric expression of certain core proteins (Strutt, 2002). In the wing, Van Gogh and Prickle localize to the proximal side of the cell, while Frizzled, Dishevelled, and Diego are enriched distally where the actin-rich trichome forms. Asymmetric protein-containing membrane domains on adjacent cells interact to regulate global alignment of trichome polarity in relation to the wing axes. Unlike fly proteins, asymmetric expression of vertebrate core PCP proteins has proven challenging to demonstrate. In polarized non-migrating neuroectoderm or axial mesoderm, fluorescent fusion proteins for Vangl2 and Prickle are enriched at anterior cell boundaries, while Dishevelled preferentially localizes to posterior membranes (Ciruna et al., 2006; Roszko et al., 2015; Yin et al., 2008). It is unknown whether PCP proteins are asymmetrically expressed in lateral ectodermal or mesodermal cells undergoing directed migration. Data from non-migrating cells suggest an anterior/posterior axis of PCP. However, migrating gastrula cells exhibit dynamic changes in cell shape, orientation, and position relative to neighboring cells (Jessen et al., 2002; Roszko et al., 2015; Yin et al., 2009) and a plane of polarization may be difficult to discern. Whatever the subcellular distribution of PCP proteins, understanding their function in migrating gastrula cells remains a key question.

For migrating cells, adhesion to the extracellular matrix (ECM) is usually required to generate traction needed for membrane protrusion formation and cell body translocation (Friedl and Gilmour, 2009). During migration, *vangl2* mutant cells lack directionality, indicating a possible relationship between Vangl2, the ECM, and membrane-protrusive activity. Experiments using the frog gastrula demonstrate that integrin α5β1 and fibronectin interactions suppress inappropriate membrane-protrusive activity (Davidson et al., 2006). Moreover, overexpression of frog Vangl2, Prickle, or Frizzled7 disrupts fibronectin fibril assembly and organization, in a manner correlating with the severity of the PCP phenotype (Goto et al., 2005). Similar to frog gastrulation movements, zebrafish convergence and extension occur in the context of a fibronectin-containing ECM network (Boucaut and Darribere, 1983; Latimer and Jessen, 2010; Winklbauer and Keller, 1996). During gastrulation a layer of fibronectin forms between the ectoderm and superficial mesoderm and another layer between the yolk and mesendoderm with individual fibrils protruding between cells (Latimer and Jessen, 2010). Therefore by late gastrulation ectodermal and mesodermal cell migration is associated with a fibrillar ECM. Notably while loss of either Vangl2 or Prickle1a results in reduced fibronectin, *glypican4* mutant embryos exhibit increased fibronectin assembly (Dohn et al., 2013; Williams et al., 2012). These different effects on

ECM structure further support the notion that Vangl2/Prickle1a and Glypican4/PCP signaling have distinct effects on cell behaviors. In addition, these data suggest fibronectin may be necessary for certain aspects of Vangl2 function.

The major goal of this study was to determine how Vangl2 and fibronectin regulate membrane protrusion dynamics in migrating zebrafish gastrula cells. We used time-lapse imaging combined with mosaic expression of fluorescent fusion proteins to visualize protrusions in live embryos. We show Vangl2 regulates distinct aspects of protrusion formation compared to Glypican4. We find GFP-VANGL2 expression to be generally symmetric in migrating gastrula cells but enriched in forming membrane protrusions compared to non-protrusive domains. Our work implicates fibronectin in the regulation of protrusion formation and polarization, and Vangl2 cell surface expression. Finally, we show increasing fibrillar fibronectin in *vangl2* mutant embryos rescues the protrusion phenotype but not PCP. These results uncover a previously unrecognized interaction between Vangl2, fibronectin, and membrane-protrusive activity required for the dorsal convergence of gastrula cells.

RESULTS

Vangl2 and Glypican4 differentially regulate membrane protrusion formation and directed migration

Multiple cell behaviors contribute to the processes of convergence and extension during zebrafish gastrulation, including the directed migration of lateral cells toward the dorsal body axis (Jessen and Solnica-Krezel, 2005). While wild-type gastrula cells are elongated and mediolaterally aligned, this type of PCP is disrupted in *vangl2* and *glypican4* homozygous mutant embryos (Jessen et al., 2002; Topczewski et al., 2001). To better understand the mechanism whereby Vangl2 regulates dorsal convergence, we analyzed and compared membrane protrusion formation in *vangl2*$^{m209/m209}$ and *glypican4*$^{m119/m119}$ mutants. Time-lapse confocal microscopy was used to image late gastrula lateral ectodermal cells 40-60 degrees from the notochord (Fig. 1A). We achieved mosaic labeling by injecting single blastomeres from 8-cell stage embryos with synthetic mRNA encoding fluorescent fusion proteins. Lifeact-GFP and membrane-targeted RFP (memRFP) were used to assess the types of membrane protrusions formed by lateral ectodermal cells. Three distinct protrusions were identified: small spike-like, actin-rich protrusions resembling filopodia; large sheet-like, actin-rich protrusions resembling lamellipodia/filolamellipodia (henceforth large protrusions); and spherical bleb-like protrusions that are initially devoid of actin (Blaser et

al., 2006) (Fig. 1B,C). Filopodia-like protrusions (henceforth filopodia) predominate followed by large protrusions, and thus, were the focus of our study. Bleb-like protrusions are much less abundant and often associated with dividing cells (Fig. 1C).

For analysis of membrane-protrusive activity, single blastomeres were injected with only membrane-targeted GFP (memGFP) to minimize mRNA cytotoxicity. Homozygous *vangl2* and *glypican4* mutant embryos are identified by their strong convergence and extension phenotypes at tailbud stage (Fig. 2A) (Solnica-Krezel et al., 1996). First, we confirmed that mutant lateral ectodermal cells have defective PCP as indicated by a reduced length-width-ratio (LWR) and MLA (Fig. 2B). We next quantified the number of protrusions formed by ectodermal cells. Wild-type embryos average 13.16 filopodia and 3.68 large protrusions per cell (Fig. 2C-E). In *vangl2* embryos, these averages increase to 24.84 filopodia and 5.77 large protrusions per cell (Fig. 2C-E). By contrast, *glypican4* mutant ectodermal cells have no difference in the number of filopodia (9.58) or large protrusions (3.59) compared to wild type (Fig. 2C-E). From the total number of large protrusions, we determined the proportion that are productive, meaning protrusion formation in one direction is followed by cell body translocation in the same direction. We find the average number of productive protrusions formed by cells in *vangl2* and *glypican4* embryos to be increased (Fig. 2F; wild type=1.58, *vangl2*=2.50, *glypican4*=2.92).

Given the difference in protrusion number between *vangl2* and *glypican4* mutant embryos, we examined the polarity of filopodia and large protrusions. Similar to MLA, protrusion polarity was determined in relation to the notochord running anterior-posterior along the dorsal body axis. Protrusions were considered polarized if their base was oriented ±45^{o} from the path of dorsal migration and included protrusions at both the leading and trailing edges (Fig. 3A). We did not detect a polarized distribution of filopodia in ectodermal cells (Fig. 3B; wild type=53.23%, *vangl2*=49.52%, *glypican4*=54.27% polarized protrusions). However, there is a significant difference between the numbers of leading versus trailing edge wild-type filopodia (Fig. 3C; 32.97% and 20.26%, respectively). We also found that a decreased number of *vangl2* mutant filopodia localized to the trailing edge compared to wild type (Fig. 3C; *vangl2*=21.69%). Unlike filopodia, 73.10% of wild-type large protrusions are oriented along the path of dorsal migration (Fig. 3D). By contrast, a reduced number of polarized large protrusions are observed in ectodermal cells from both *vangl2* and *glypican4* mutant embryos (Fig. 3D; *vangl2*=43.76%, *glypican4*=50.97%). We detected no difference in the numbers of leading versus trailing edge large protrusions in wild type or PCP mutant embryos (Fig. 3E). Rose diagrams indicate that *vangl2* and *glypican4* mutant ectodermal cells

generate large protrusions at multiple positions around their circumference (Fig. S1). The reduced number of polarized large protrusions in *vangl2* and *glypican4* mutant ectoderm suggests these cells have indirect migration trajectories. Migration directness values were calculated by dividing the Euclidean distance by the accumulated or total migration distance (Table S1); a value of one indicates a straight migration path. While *vangl2* mutant ectodermal cells have reduced directness (0.83) compared to wild type (0.96), loss of Glypican4 function has a negligible effect (0.94) on directness (Fig. 3F). However, trajectory plots indicate that both mutations disrupt overall net dorsal convergence (Fig. 3G). These data imply that Vangl2 and Glypican4 are both necessary for PCP and polarized membrane-protrusive activity, but these proteins have distinct effects on protrusion formation and directed cell movement.

Vangl2 overexpression affects membrane-protrusive activity similar to loss of Vangl2

Another hallmark of core PCP protein function is that excess activity results in cell polarity defects (Yang and Mlodzik, 2015). Previously published work has not reported Vangl2 overexpression relative to Vangl2 loss of function cellular phenotypes. Therefore we performed Vangl2 gain of function studies to substantiate its role in membrane protrusion formation and polarity. We verified *vangl2* mRNA injection at the single-cell stage increases protein expression with immunofluorescence (Fig. S2) and western blot (Fig. S3) and. We used live imaging and whole-mount *in situ* hybridization to visualize the severity of the convergence and extension phenotype at the end of gastrulation. Compared to controls, *vangl2*-injected wild-type embryos are broadened mediolaterally and have shorter anterior-posterior axes (Fig. S3). Next, using mosaic memGFP expression and time-lapse imaging, we analyzed PCP and membrane protrusions in *vangl2*-injected embryos. Again, *vangl2* mRNA injection was done at the single-cell stage to promote ubiquitous protein expression. The LWRs and MLA of *vangl2* overexpressing lateral ectodermal cells are reduced compared to wild type (Fig. S3). Increased Vangl2 causes lateral ectodermal cells to average twice as many filopodia (27.63) and large protrusions (6.44) as control cells (Fig. S3). Vangl2 overexpression also disrupts filopodium and large protrusion polarity (Fig. S1; Fig. S3; 40.74% and 49.64% polarized protrusions, respectively). Lastly, increasing Vangl2 protein levels has a strong effect on directed ectodermal cell migration (Fig. S3; wild type=0.96, *vangl2* mRNA=0.69). These results indicate that a specific level of cell surface Vangl2 expression is essential for PCP, membrane-protrusive activity, and directed migration.

Vangl2 expression is enriched in forming membrane protrusions

Previous work using polarized zebrafish notochord cells demonstrates asymmetric, anterior membrane-biased Vangl2 protein expression at post-gastrulation stages (Roszko et al., 2015). Axial cells are unlike lateral gastrula cells engaged in directed migration in terms of dynamic changes in membrane-protrusive activity and position relative to neighboring cells. Therefore we examined the distribution of a human GFP-VANGL2 fusion protein (Roszko et al., 2015) in anterior, posterior, leading edge, and trailing edge plasma membrane domains of wild-type lateral ectodermal cells. Here, anterior/posterior refers to the cell axis perpendicular to the path of dorsal migration, while the leading edge/trailing edge axis is parallel to the migration path (Fig. S4). Single blastomeres from 8-cell stage embryos were injected with synthetic mRNA encoding GFP-VANGL2 to generate mosaic expression, and cells were imaged at the tailbud-1-somite stage. We injected GFP-VANGL2 at low doses so as not to perturb cell polarity (Roszko et al., 2015). Blastomeres were co-injected with memRFP to control for plasma membrane variations and changes in fluorescence intensity due to membrane thinning or thickening. Consistent with published data (Roszko et al., 2015), GFP-VANGL2 localizes in a punctate pattern at the plasma membrane and within putative vesicular compartments (Figs S4, 4A). By analyzing the fluorescence intensity ratios at multiple positions along the anterior to posterior membrane domains, we conclude GFP-VANGL2 expression is not broadly asymmetric in polarized lateral ectodermal cells (Fig. S4). Similar results were obtained for the leading edge and trailing edge membrane domains (Fig. S4).

The increased number of membrane protrusions in *vangl2* mutant cells suggests Vangl2 may normally function to inhibit protrusive activity or limit protrusion formation or lifespan at specific membrane domains. Therefore, we quantified GFP-VANGL2 protein expression during the formation of large protrusions. Large protrusions were chosen because they are associated with migratory behaviors, like cell body translocation. We quantified fluorescence intensity at three subjectively named time points: prior to protrusion formation (preparation phase); during early protrusion development (eruption phase); and after protrusion elongation or remodeling (extension phase). Blastomeres were injected with a combination of GFP-VANGL2 and memRFP, and time-lapse imaging was performed near the tailbud stage (Fig. 4A). We report a significant increase in GFP-VANGL2 protein localization within erupting membrane protrusions (Fig. 4B,C) that becomes reduced as protrusions extend or remodel (Fig. 4B,D). GFP-VANGL2 expression within erupting protrusions is enriched compared to non-protrusive membrane domains (Fig. S5). However, our studies find no difference in GFP-VANGL2 localization between polarized and non-polarized protrusions (Fig. S5). In

conclusion, while GFP-VANGL2 does not exhibit widespread asymmetric membrane expression in migrating gastrula cells, our data demonstrate protein enrichment in membrane domains associated with protrusive activity.

Fibronectin is required for membrane protrusion formation and polarity

Our published data report that *vangl2* mutant embryos and *prickle1a* morphants have reduced fibronectin (Dohn et al., 2013; Williams et al., 2012). Experiments using the frog gastrula indicate integrin-fibronectin interactions are essential for polarized membrane protrusion formation (Davidson et al., 2006). Therefore we hypothesized that loss of fibronectin disrupts protrusion formation and, perhaps, PCP in lateral ectodermal cells. Zebrafish express two fibronectin genes (*fn1a* and *fn1b*) during gastrulation (Sun et al., 2005; Thisse, 2001; Trinh and Stainier, 2004). Correlating with establishment of PCP, fibronectin protein expression and fibril assembly increase near the end of gastrulation (Fig. 5A) (Latimer and Jessen, 2010; Roszko et al., 2015). We used a combination of *fn1a* and *fn1b* antisense morpholino oligonucleotides to knockdown protein expression, which produces a mild convergence and extension phenotype in wild-type embryos (Fig. 5B) (Julich et al., 2005; Latimer and Jessen, 2010). These morpholinos reduce fibronectin expression during gastrulation, a phenotype that is rescued by injection of *fn1a/1b* mRNA (Fig. S6) (Latimer and Jessen, 2010). Fibronectin knockdown alters LWRs and MLA compared to wild type but does not reduce PCP to the extent observed during Vangl2 loss of function (Figs 5C). Reduced fibronectin expression also causes ectodermal cells to have excess numbers of filopodia and large protrusions (Fig. 5D-F; 25.42 and 5.94, respectively) similar to those found in *vangl2* mutant cells. Unlike the filopodia of *fn1a/1b* morphant ectodermal cells, the percentage of polarized large protrusions is markedly lower (Fig. S1; Fig. 5E,F; 46.88% polarized protrusions). Further, loss of fibronectin disrupts the directed migration of ectodermal cells (Fig. 5G,H; wild type=0.96, *fn1a/1b* MO=0.91). These data provide evidence that fibronectin supports proper membrane-protrusive activity, but the ECM plays a lesser role during establishment of PCP and convergence and extension movements.

Fibronectin regulates cell surface Vangl2 expression

Vangl2 protein expression at the plasma membrane increases at mid-gastrulation, just prior to the onset of Vangl2-dependent PCP and appearance of the *vangl2* mutant convergence and extension phenotype (Roszko et al., 2015; Sepich et al., 2000). At mid-gastrulation, loss of Vangl2 increases the formation of large membrane protrusions but does not affect protrusion

polarity (Fig. S7). Vangl2 membrane localization and hence cell surface function is regulated by Prickle1a and an unknown extracellular signal or signals (Dohn et al., 2013; Roszko et al., 2015). As the late gastrula undergoes Vangl2-dependent changes in cell behavior, fibrillar fibronectin increases (Latimer and Jessen, 2010). Therefore we reasoned that fibronectin may control Vangl2 membrane accumulation. To determine the role of fibronectin for Vangl2 translocation to the cell surface, wild-type embryos were injected with *fn1a*/*fn1b* morpholinos and fixed for Vangl2 immunolabeling at two stages, early gastrulation (60% epiboly) and the end of gastrulation (tailbud). Vangl2 is primarily cytoplasmic during early gastrulation (Fig. S8) and translocates to the plasma membrane at mid-gastrulation stages (Roszko et al., 2015). Here, we used a polyclonal antibody recognizing an epitope near the Vangl2 N-terminus (Fig. S2). Vangl2 expression at 60% epiboly is similar between morphant and control embryos (Fig. S8). However by tailbud, Vangl2 does not localize effectively to the plasma membranes of ectodermal (Fig. 6A,B) or mesodermal cells (Fig. 6C,D) in *fn1a/1b* morphants. Though the immunofluorescence images suggest reduced cell surface Vangl2 expression could be attributed to protein loss, western blot analyses indicate morphant embryos have near normal levels of Vangl2 protein (Fig. S9). Together, these data are evidence that fibronectin is necessary for Vangl2 translocation to the plasma membrane and suggest the *fn1a/1b* morphant phenotype may partially be due to loss of Vangl2 at the cell surface.

Fibronectin rescues membrane-protrusive activity but not PCP in *vangl2* mutant embryos

The ability of fibronectin to promote cell surface Vangl2 expression indicates a complex relationship between the ECM, PCP, and formation of polarized protrusions. This is supported by our *in vitro* data implicating human VANGL2 in regulation of integrin-mediated cell adhesion to multiple ECM proteins (Jessen and Jessen, 2017). Loss of Vangl2 decreases fibronectin protein and fibril assembly (Williams et al., 2012) and morpholino knockdown of fibronectin in *vangl2* mutant embryos does not enhance the protrusion phenotypes (Fig. S10). Similarly, *vangl2* mRNA overexpression in *fn1a/1b* morphant embryos does not enhance the individual protrusion phenotypes (Fig. S11). To further elucidate the relationship between fibronectin and Vangl2, we tested whether an increase in fibronectin suppresses the protrusion phenotypes in *vangl2* mutants. We injected single-cell stage embryos with an equal mixture of synthetic mRNA encoding *fn1a* and *fn1b*. Both *fn1a/1b* mRNA-injected *vangl2* mutant and wild-type embryos have increased fibronectin, but *vangl2* mutants, in particular, have increased fibrillogenesis (Fig. 7A). In addition to

fn1a/*1b* mRNA, embryos were injected with memGFP at the 8-cell stage to achieve mosaic labeling and cells were imaged using time-lapse microscopy. Ectodermal cells from *fn1a/1b*-injected *vangl2* mutants have near wild-type numbers of filopodia and large membrane protrusions (Fig. 7B-D; 15.69 and 4.13, respectively). Despite the rescue of protrusion number, injected *vangl2* mutant embryos retain the convergence and extension phenotype seen in control embryos (Fig. S12). Therefore, we further examined membrane protrusion polarity and the PCP of ectodermal cell bodies. Total filopodia polarity is unaffected in *vangl2* mutant embryos, which remains unchanged in *fn1a/1b*-injected mutants (Fig. 7C). Defective polarization of large protrusions in *vangl2* mutants was partially rescued by increasing fibronectin expression (Fig. S1; Fig. 7D; 54.37% polarized protrusions). By contrast, neither the elongation nor orientation of *vangl2* mutant ectodermal cells was improved (Fig. 7E). Nonetheless, increasing fibronectin in *vangl2* mutant embryos rescues the directed migration phenotype (Fig. 7F,G). These data confirm PCP is required for convergence and extension movements and illustrate that ECM supports proper membrane-protrusive activity and directed cell migration. Fibronectin however, is not sufficient for establishment of PCP.

DISCUSSION

PCP proteins are linked to several morphogenetic processes, including the gastrulation movements of convergence and extension (Gray et al., 2011). At ~80% epiboly lateral gastrula cells engage in directed migration behaviors, which continue through tailbud stage (Sepich et al., 2005). As they migrate, round cells elongate and mediolaterally align (Roszko et al., 2015). This event is accompanied by a straightening of migration trajectories toward the dorsal axis, a process failing to occur in *vangl2* mutant embryos (Jessen et al., 2002). In the fly wing, core PCP proteins regulate the production and asymmetric positioning of a single actin-rich trichome in each epithelial cell (Strutt and Strutt, 2007; Taylor et al., 1998). Thus regulation of actin rearrangements is thought to underlie establishment of PCP in vertebrate tissues. However, it was not clear whether PCP proteins regulate actin-rich membrane protrusions in migrating lateral gastrula cells. We systematically analyzed formation and polarization of protrusions in cells with disrupted Vangl2 function and compared these phenotypes with those obtained after manipulation of Glypican4/PCP signaling. We define cellular domains of Vangl2 protein expression and report Vangl2 enrichment at the cell surface requires fibronectin. We establish a role for the ECM during protrusion formation and polarization and link fibronectin with Vangl2 function.

Regulation of membrane-protrusive activity by PCP proteins

During early zebrafish gastrulation before the onset of PCP-dependent cell movements, dorsal prechordal plate progenitor cells use a combination of blebs and actin-containing filopodia and large lamellipodia-like protrusions (Diz-Munoz et al., 2010). Here, large protrusions are associated with directed migration and blebs with cell tumbling and meandering (Diz-Munoz et al., 2016). Using time-lapse imaging and mosaic memGFP expression, we examined for the first time dynamic membrane-protrusive activity occurring as polarized lateral ectodermal cells undergo directed migration. Our analysis identified filopodia and large protrusions as the predominant protrusions produced by ectodermal cells. Blebs are less abundant, except in dividing cells where they form at cell poles to stabilize cell shape (Sedzinski et al., 2011).

Ectodermal cells with loss of Vangl2 but not loss of Glypican4 have increased numbers of filopodia and large protrusions. Glypican4 likely acts as a Wnt co-receptor to activate downstream proteins and, subsequently, actin regulators (Roszko et al., 2009). By contrast, Vangl2 interacts with Prickle1a to potentially contain or limit Glypican4/PCP signaling within specific cellular domains. While the *vangl2* and *glypican4* mutant convergence and extension phenotypes are similar, our data assert these proteins have distinct effects on the ECM. In *glypican4* mutant embryos, fibrillar fibronectin is enhanced due to increased cell surface cadherin expression and cell adhesion (Dohn et al., 2013). Conversely, *vangl2* mutant and *prickle1a* morphant embryos exhibit decreased fibronectin expression and assembly, possibly due to increased matrix metalloproteinase activity and/or decreased cadherin expression (Dohn et al., 2013; Williams et al., 2012). We propose that fibronectin is necessary for proper formation and polarization of membrane protrusions (see further discussion below). Consequently, while increased in *vangl2* mutant embryos, protrusion number is not higher in *glypican4* mutants, as the fibronectin ECM remains intact. The ability of fibronectin to function as a suppressor of excess protrusion formation is supported by previous work in frog (Davidson et al., 2006).

Notably, *vangl2* and *glypican4* deficient ectodermal cells have excess non-polarized large protrusions, suggesting a relationship between protrusion polarity and establishment of PCP. Previous work reports *vangl2* mutant mesodermal cell MLA is slightly biased along the anterior/posterior axis (Roszko et al., 2015). While rose diagrams suggest a slight anterior/posterior bias in the polarization of large protrusions from *vangl2* and *glypican4* mutant ectodermal cells, in general, protrusions were detected around the entire cell

circumference. These data support the notion that loss of protrusion polarity may represent an expansion of membrane domains capable of forming protrusions. A bias in wild-type filopodia polarity was not detected, indicating these thin protrusions may play a sensory role. After surveying the extracellular environment for specific signals, we hypothesize that filopodia promote polarized large lamellipodia-like protrusion formation (Faix and Rottner, 2006). When wild-type lateral gastrula cells migrate dorsally, they generate more cell-cell contacts as they align and pack. One assumption is that mediolaterally oriented protrusions aid cell packing and thus directed movement. As a result, individual cell behaviors would affect morphogenesis at the tissue level (Davidson et al., 2010). Additionally, manipulation of Vangl2 function interferes with ectodermal cell directed movement. Despite having a protrusion polarity phenotype similar to that found in *vangl2* mutant embryos, *glypican4* mutant cells migrate along relatively straight trajectories, indicating polarized-protrusive activity may not be sufficient for directed migration. Unlike *vangl2* mutant embryos however, *glypican4* mutants have normal numbers of membrane protrusions and both increased cadherin-mediated cell adhesion and increased fibronectin fibrillogenesis (Dohn et al., 2013). We hypothesize that these features contribute to more efficient directed migration of ectodermal cells in *glypican4* mutant embryos compared to *vangl2* mutants. The mechanism behind Glypican4/PCP signaling and its effects on cell packing and migration trajectories need to be further explored, as directed mesodermal cell migration is also Vangl2-dependent (Jessen et al., 2002).

Vangl2 expression in migrating ectodermal cells

A feature of fly PCP, certain core proteins are asymmetrically expressed in the wing epithelium (Strutt and Strutt, 2009). Fluorescent fusion proteins and cell transplantation methods allowed identification of an anterior/posterior axis of asymmetric PCP protein expression in non-migratory polarized axial cells. Here, Vangl2 and Prickle are enriched at anterior membranes, while Dishevelled localizes posteriorly (Ciruna et al., 2006; Roszko et al., 2015; Yin et al., 2008). It is important to note axial cells do not exhibit Vangl2 or Prickle asymmetry in gastrula-stage embryos (Roszko et al., 2015; Yin et al., 2008). Based on our examination of lateral ectodermal cells engaged in directed migration, GFP-VANGL2 does not localize asymmetrically along either the anterior/posterior or leading edge/trailing edge cell axes. These cells undergo rapid changes in morphology and cohesiveness as they migrate and because Vangl2 expression is dynamic in migrating cells, an asymmetry may remain undetected. It is possible that subtle differences in Vangl2 protein stability exist at certain

regions of the membrane (Chien et al., 2015). Our data do confirm that GFP-VANGL2 is enriched at plasma membrane domains engaged in protrusive activity compared to non-protrusive domains. Specifically, GFP-VANGL2 expression exhibits a transient increase within newly developed large protrusions prior to protrusion elongation or remodeling. These data are reminiscent of zebrafish hindbrain motor neurons where GFP-Vangl2 expression localizes to filopodia tips before protrusion retraction (Davey et al., 2016). Our study did not find a difference in GFP-VANGL2 expression between polarized and non-polarized protrusions. Wild-type ectodermal cells form protrusions around their circumference but produce more that are polarized along the path of migration. By contrast, *vangl2* mutant cells have both an increased number of protrusions and an increased number of non-polarized protrusions. We hypothesize that, rather than acting as a general inhibitor of membrane protrusion formation, Vangl2 acts to destabilize, restrict, or limit protrusive activity. Further work is needed to determine how Vangl2 expression and function are regulated at distinct membrane domains and how this translates into polarized cell behaviors. For example, Prickle1a may influence subtle differences in Vangl2 expression or stability at polarized versus non-polarized protrusions. Notably, *vangl2* mRNA overexpression does not inhibit protrusion formation suggesting that a balanced level of core PCP protein expression is necessary for proper protrusive activity and directed migration. Perhaps Vangl2-dependent communication of signals within and between cells regulates localization of other PCP proteins to membrane protrusions (Strutt and Strutt, 2009).

At early gastrulation, Vangl2 protein localizes within presumptive cytoplasmic vesicles but enriches at the plasma membrane by mid-gastrulation. Vangl2 cell surface expression at mid-gastrulation precedes the Vangl2-dependent onset of PCP and protrusion polarization. Our previous work demonstrates Prickle1a can control Vangl2 expression (Dohn et al., 2013), suggesting that *prickle1a* morphant phenotypes may be partially due to disrupted Vangl2 function. Interestingly, disruption of other polarity proteins (Glypican4, Frizzled7, Dishevelled, and Scribble1) or tissue patterning regulators does not significantly affect cell surface Vangl2 expression (Roszko et al., 2015). Because of a temporal correlation between the requirement for Vangl2 and fibronectin fibrillogenesis at late gastrulation (Latimer and Jessen, 2010; Sepich et al., 2000), we hypothesized that the ECM influences plasma membrane levels of Vangl2. We report that loss of fibronectin inhibits translocation to the membrane, but whether fibronectin impacts Vangl2 expression directly or indirectly is unclear. Human VANGL2 interacts with integrin αv and promotes cell adhesion to ECM

substrates, including fibronectin (Jessen and Jessen, 2017). We hypothesize that integrin-fibronectin interactions may affect Vangl2 protein stability and function at the plasma membrane. Other signaling pathways or post-translational modifications may also contribute to Vangl2 intracellular trafficking and expression (Gao et al., 2011; Merte et al., 2009).

Interaction of fibronectin and Vangl2 during protrusion formation and polarization

Fibronectin is long recognized for its roles in vertebrate gastrulation. Among these, fibronectin affects cell polarity and protrusive activity, as well as, provides a substrate or tracks for migration (Darribere and Schwarzbauer, 2000; Davidson et al., 2006; Winklbauer and Keller, 1996). However, the requirement for fibronectin during zebrafish gastrulation and its relationship with PCP protein function are still emerging. Lateral ectodermal cells interact with a network of fibronectin and laminin, which forms a boundary at the ectoderm/mesoderm interface (Latimer and Jessen, 2010). Laminin mutant embryos do not have obvious gastrulation cell movement phenotypes (Parsons et al., 2002). Assembly of fibronectin fibrils relies on actin mechanotension generated by integrin-mediated cell-matrix interactions and cadherin-mediated adhesion (Schwarzbauer and DeSimone, 2011). We now show that *fn1a/1b* morphant embryos have defects in PCP and membrane protrusion number and polarity. While the protrusion phenotypes are similar to those of *vangl2* mutant embryos, loss of fibronectin has a lesser effect on MLA and directed cell migration. We hypothesize that the ECM is not essential for all cell behaviors underlying dorsal convergence and, further, reduced fibronectin in *vangl2* mutant gastrulae is not sufficient to explain the severity of the *vangl2* phenotype. Supporting this notion, neither zygotic *fn1a/natter* mutant embryos (Trinh and Stainier, 2004) nor *fn1a/1b* morphants (Latimer and Jessen, 2010) exhibit strong convergence and extension defects. Moreover, the *vangl2* cell elongation, MLA, and gastrulation phenotypes cannot be rescued by increasing fibronectin. Loss of Vangl2 increases matrix metalloproteinase activity and decreases cell surface cadherin expression (Cantrell and Jessen, 2010; Dohn et al., 2013; Jessen and Jessen, 2017; Williams et al., 2012), either of which compromises the ability to assemble a normal ECM. Although fibronectin expression cannot be restored to wild-type levels in *vangl2* mutant embryos, *fn1a/fn1b* mRNA rescues protrusion number, directed migration, and to a lesser extent protrusion polarity. It is unclear how a uniform fibronectin ECM promotes polarized protrusive activity given that GFP-VANGL2 localizes to both polarized and non-polarized protrusions. It will be important to understand in more detail the dynamics of Vangl2 expression in polarized gastrula cells and to determine the localization patterns of other core PCP proteins. Our

results indicate fibronectin is required to suppress excess protrusion formation. Moreover, we argue fibronectin regulates protrusion number and polarity directly, but by inhibiting cell surface Vangl2 expression it influences PCP indirectly. The ability of Vangl2 to affect fibronectin proteolysis and cadherin expression (Dohn et al., 2013; Williams et al., 2012) provide possible mechanisms to regulate ECM assembly, and subsequently, membrane-protrusive activity. Future studies will further address the complex relationships between Vangl2 function, Glypican4/PCP signaling, and the fibronectin ECM.

MATERIALS AND METHODS

Zebrafish lines and husbandry

Adult zebrafish (*Danio rerio*) 1-2 years of age were maintained following standard procedures (Solnica-Krezel et al., 1994). Embryos were collected after natural spawning, grown at 28.5ºC in egg water (purified water with 60 mg/L Instant Ocean), and staged according to morphology (Kimmel et al., 1995). Embryo ages were between 6 and 10.5 hours post-fertilization. Strains used in this study included the following: wild type (AB*, TL, and WIK), *vangl2*/*trilobite*^{m209} (Jessen et al., 2002; Solnica-Krezel et al., 1996), *vangl2*/*trilobite*^{vu7} (Jessen et al., 2002), and *glypican4*/*knypek*^{m119} (Solnica-Krezel et al., 1996; Topczewski et al., 2001). The *vangl2*^{m209} and *glypican4*^{m119} alleles behave like null mutations while the *vangl2*^{vu7} allele is a chromosomal deletion lacking the *vangl2* gene.

The Middle Tennessee State University Institutional Animal Care and Use Committee approved the animal research described in this paper. All procedures were conducted following approved guidelines. The Office of Laboratory Animal Welfare assurance number is A4701-01.

Morpholinos, synthetic mRNA, and embryo microinjection

Antisense morpholino oligonucleotides were obtained from Gene Tools, LLC. The following previously published morpholinos were used: *fn1a* (5'-tttttcacaggtgcgattgaacac-3'), *fn1b* (5'-tactgactcacgggtcattttcacc-3' and 5'-gcttctggctttgactgtatttcgg-3'), and *vangl2* (5'-agttccaccttactcctgagagaat-3') (Dohn et al., 2013; Julich et al., 2005; Latimer and Jessen, 2010; Trinh and Stainier, 2004; Veeman et al., 2003; Williams et al., 2012). Each morpholino was injected at a dose of 3-10 ng/embryo. The *fn1a/1b* morpholino combination reduces fibronectin protein expression (Fig. S3) and produces the reported anterior somite defect (Julich et al., 2005; Koshida et al., 2005; Latimer and Jessen, 2010). The *vangl2* morpholino produces convergence and

extension phenotypes (Dohn et al., 2013; Williams et al., 2012) and late gastrulation ectodermal cell protrusion phenotypes similar to the *vangl2*$^{m209/m209}$ mutant (24.60 filopodia and 5.77 large protrusions on average per cell). None of the morpholinos used in this study stimulate obvious p53-dependent cell death.

DNA-encoding full-length Vangl2, the F-actin marker Lifeact-GFP (Riedl et al., 2008), memGFP, memRFP, GFP-VANGL2, Fibronectin 1a, and Fibronectin 1b were cloned in the pCS2 vector and linearized by *NotI* restriction endonuclease. The *fibronectin* clones are not targeted by the *fn1a/1b* morpholinos. Synthetic mRNA was made using the Sp6 mMessage mMachine kit as directed by the manufacturer (Ambion) and purified by G-50 sephadex columns (Roche). Microinjection into single-cell stage or 8-cell stage embryos was performed following standard methods (Gilmour, 2002). Synthetic mRNA was injected at the following doses: *vangl2* (100-300 pg); *Lifeact-GFP* (100 pg), *memGFP* and *memRFP* (100 pg); *GFP-VANGL2* (50 pg); *fn1a* and *fn1b* (200 pg).

Whole-mount *in situ* hybridization, immunofluorescence, and antibodies

Staged embryos were fixed overnight in 4% paraformaldehyde in PBS and washed with PBS containing 0.1% Tween-20 before high resolution *in situ* hybridizations were performed as described (Thisse and Thisse, 2008). Antisense RNA probes were generated by *in vitro* transcription and purified following standard methods (Westerfield, 2000). For immunofluorescence, embryos were fixed in either 4% paraformaldehyde/PBS/sucrose fix buffer (1:1 mixture of 8% paraformaldehyde/PBS and 2X sucrose buffer; 8.0 g Sucrose, 0.15 ml 0.2 M $CaCl_2$, 90 ml 0.2 M Na_2HPO_4 buffer, pH 7.3) overnight or in Prefer fixative (Anatech Ltd.) for 2 h, and then manually dechorionated and permeabilized for 30 min at room temperature (5% normal donkey serum, 0.5% Triton, PBS). Embryos were blocked 2 h at room temperature (5% BSA, 1% DMSO, 0.1% Triton, PBS) with gentle rocking. Primary antibodies diluted in block solution at 1:100 were applied before incubating embryos overnight at 4°C with gentle rocking. Embryos were washed six times, 15 min each, in PBST with DMSO (0.1% Triton, 1% DMSO, PBS). Embryos were treated with secondary antibodies (Jackson ImmunoResearch), diluted 1:500 in 50% block and 50% PBST (0.1% Triton, PBS), and incubated 2 h at room temperature under UV protection with gentle rocking. For nuclei labeling, embryos were washed with PBS prior to 30 min incubation in DAPI (2-(4-amidinophenyl)-1H - indole-6-carboxamidine). Embryos were washed three times with PBS and stored at 4°C.

Sections were obtained by embedding fibronectin immunolabeled/DAPI stained embryos in 1.2% agarose in a 5% sucrose solution followed by cryosectioning (10 μm). Fibronectin was detected using a rabbit polyclonal antibody generated against an epitope within the human protein (F3648, Sigma-Aldrich). An affinity purified rabbit polyclonal antibody capable of recognizing an epitope near the N-terminus (NH_2-RSKSRDSSSRGDKSC-COOH) of zebrafish Vangl2 was generated (ProSci Inc.). This antibody will not bind Vangl1 due to lack of epitope sequence homology, and Vangl1 is not expressed during gastrulation (Jessen and Solnica-Krezel, 2004). We validated the antibody by immunolabeling embryos overexpressing *vangl2* mRNA and embryos with a *vangl2* chromosomal deletion (Fig. S2).

Embryo protein extraction, western blot, and antibodies

For zebrafish embryo whole-cell lysates, pools of approximately 20-50 embryos were manually dechorionated, deyolked, lysed in RIPA (50 mM Tris, pH 7.4, 150 mM NaCl, 1% NP-40, 0.5% DOC, 0.1% SDS, mammalian protease inhibitor cocktail), and clarified by centrifugation. Whole-embryo lysates were boiled 10 min following addition of Laemmli sample buffer (1x final concentration). Protein extracts were separated by 10% SDS-PAGE and transferred to PVDF membrane using a trans-blot turbo transfer system following the manufacturer's instructions (Bio-Rad). Non-specific binding to membranes was blocked with 5% non-fat milk in TBS-Tween (50 mM Tris, pH 7.4, 150 mM NaCl, 0.1% Tween-20), and membranes incubated overnight with rabbit polyclonal Vangl2 antibody (1:1,000) in block at 4°C with gentle rocking. Membranes were incubated with a peroxidase-conjugated secondary antibody (1:5,000; Jackson ImmunoResearch), developed using Clarity ECL substrate (Bio-Rad), and imaged using a UVP GelDoc-It Imaging System (Upland, CA). During each experiment blots were stripped at room temperature for 15 min using 25 mM glycine and 1% SDS (pH 2.0) and re-probed in a 1:1,000 dilution of beta-actin antibody (#4967, Cell Signaling Technology). Densitometry was performed on western blots with UVP Visionworks software.

Microscopic imaging

Staged and dechorionated live or fixed embryos were mounted as previously described (Roszko et al., 2015) and imaged with a Zeiss LSM700 confocal microscope with a 63x oil-immersion objective (N.A. 1.4). Time-lapse images were collected for 20 min at 1-2

min intervals with a 0.39 or 0.50 µm z-axis step size. Embryo orientation was documented for each time-lapse series by taking low-magnification (10x) reference images under transmitted light. Yolk-plug closure-tailbud stage live embryo images were obtained with an Olympus SZX16 stereomicroscope equipped with a Q-Color5 CCD camera. Sectioned embryo images were acquired using an Olympus IX83 inverted microscope equipped with a 20x objective and a Hamamatsu Flash 4.0 CMOS camera.

Quantitation of cell shape, alignment, velocity, and directness

Cell LWRs and MLA analyses were performed using Fiji software (https://fiji.sc/) (Schindelin et al., 2012) as described (Jessen et al., 2002). To obtain cell migration velocity and directionality data, we tracked cell movement during our 20 min time-lapse image series (10 frames) using Fiji's Manual Tracking tool. This tool outputs data points distributed as scaled latitude and longitude values, which were exported to Ibidi's Chemotaxis and Migration Tool standalone software (https://ibidi.com) to generate plot diagrams and directness and velocity statistics.

Analysis of membrane protrusions

We quantified and annotated membrane protrusions using Fiji software. Protrusion number and polarity were quantified as the number formed during a 20 min time interval (10 image frames). A spike-like structure distinguished actin-rich filopodia from other types of protrusions. Large actin-rich protrusions were subjectively classified by their irregular shapes and base widths >2.5µm and included lamellipodia-like protrusions and filolamellipodia. Characterized by their spherical appearance, blebs were rare in lateral ectodermal cells. Productive protrusions were quantified as the number of large protrusions formed that were associated with cell body translocation during a 20 min time interval (10 image frames). Protrusions were classified as polarized if they had a base to tip orientation within ±45° of the path of migration. Rose diagrams were generated using the angles of individual ectodermal cell large protrusions.

GFP-VANGL2 and Vangl2 localization

Time-lapse confocal image series were collected at the tailbud-1-somite stage as described above. Prior to analysis, we subtracted the image background and created sum slice projections. For the GFP-VANGL2 localization studies, we used Fiji's Plot Profile

tool to quantify fluorescence intensities along the length of a line and generate an output of distance in μm (x-value) and grey value (y-value). To test for asymmetric membrane expression bias, we drew a line through each cell from either anterior to posterior or leading edge to trailing edge membranes before producing a plot profile. During our membrane domain fluorescence intensity analysis, we avoided membrane-protrusive domains. We selected peak values at multiple positions for each membrane domain to generate anterior/posterior and leading edge/trailing edge fluorescence intensity ratios for memRFP and GFP-VANGL2. To assess GFP-VANGL2 expression dynamics in large membrane protrusions, we used Fiji's Plot Profile tool to gather fluorescence intensity data. Drawing a line inward from the plasma membrane at three time points, the Plot Profile tool produced plot profile data similar to that of our Vangl2 asymmetry study. Because membrane protrusion cycles of gastrula cells are highly dynamic in space and time, we examined GFP-VANGL2 expression at subjective time points associated with membrane protrusion preparation, eruption, and extension. We selected the eruption plot apex, and the fluorescence intensity values for the corresponding distance points (x-values) were collected for the preparation and extension phases. These data points produced eruption/preparation and extension/eruption fluorescence intensity ratios for both memRFP and GFP-VANGL2. We used the eruption phase of large protrusion formation for comparison of GFP-VANGL2 expression between protrusive and non-protrusive domains and between polarized and non-polarized protrusions. To analyze endogenous zebrafish Vangl2 expression, we collected confocal z-stack images of epiblast cells at 60% epiboly and ectodermal and mesodermal cells at tailbud stage. We drew a line across the center of each cell from anterior to posterior membranes, and using Fiji's Plot Profile tool we generated a grey value plot profile, representative of fluorescence intensities along the length of the drawn line. Since we used Vangl2 antibody labeling and not mosaic expression, we could not discern adjacent cell membranes. For consistency, we used congruent techniques when performing plot profile analyses on control and experimental cells. The fluorescence intensities for each distance point along the drawn line were averaged to generate a mean grey value plot profile.

Statistics

Data were exported to Microsoft Excel for graphing and StatCrunch software used for statistical analysis. The statistical tests performed and significance values obtained are indicated in each figure legend. The data presented are normally distributed.

Acknowledgements

We thank Alba Diz-Muñoz and Martin Bergert for the Lifeact-GFP plasmid, Anna Parnell for technical assistance, and Tammy Jessen for excellent zebrafish facility maintenance.

Competing interests

The authors declare no competing or financial interests.

Author contributions

Conceptualization: J.R.J.; Methodology: J.R.J. and A.M.L.; Validation: A.M.L.; Formal Analysis: J.R.J. and A.M.L.; Investigation: A.M.L. and D.J.P.; Resources: J.R.J.; Writing-Original Draft: J.R.J. and A.M.L.; Writing-Review and Editing: J.R.J., A.M.L., and D.J.P.; Visualization: J.R.J. and A.M.L.; Supervision: J.R.J.; Project Administration: J.R.J.; Funding Acquisition: J.R.J.

Funding

This study was funded by a grant from the National Institutes of Health (GM102356 to J.R.J.). Certain equipment items used to conduct this research were provided by Middle Tennessee State University. J.R.J., A.M.L., and D.J.P. acknowledge support from the Molecular Biosciences Ph.D. Program.

References

Blaser, H., Reichman-Fried, M., Castanon, I., Dumstrei, K., Marlow, F. L., Kawakami, K., Solnica-Krezel, L., Heisenberg, C. P. and Raz, E. (2006). Migration of zebrafish primordial germ cells: a role for myosin contraction and cytoplasmic flow. *Dev Cell* **11**, 613-27.

Boucaut, J. C. and Darribere, T. (1983). Fibronectin in early amphibian embryos. Migrating mesodermal cells contact fibronectin established prior to gastrulation. *Cell Tissue Res* **234**, 135-45.

Cantrell, V. A. and Jessen, J. R. (2010). The planar cell polarity protein Van Gogh-Like 2 regulates tumor cell migration and matrix metalloproteinase-dependent invasion. *Cancer Lett* **287**, 54-61.

Carreira-Barbosa, F., Concha, M. L., Takeuchi, M., Ueno, N., Wilson, S. W. and Tada, M. (2003). Prickle 1 regulates cell movements during gastrulation and neuronal migration in zebrafish. *Development* **130**, 4037-46.

Chien, Y. H., Keller, R., Kintner, C. and Shook, D. R. (2015). Mechanical strain determines the axis of planar polarity in ciliated epithelia. *Curr Biol* **25**, 2774-2784.

Ciruna, B., Jenny, A., Lee, D., Mlodzik, M. and Schier, A. F. (2006). Planar cell polarity signalling couples cell division and morphogenesis during neurulation. *Nature* **439**, 220-4.

Darribere, T. and Schwarzbauer, J. E. (2000). Fibronectin matrix composition and organization can regulate cell migration during amphibian development. *Mech Dev* **92**, 239-50.

Davey, C. F., Mathewson, A. W. and Moens, C. B. (2016). PCP Signaling between Migrating Neurons and their Planar-Polarized Neuroepithelial Environment Controls Filopodial Dynamics and Directional Migration. *PLoS Genet* **12**, e1005934.

Davidson, L. A., Joshi, S. D., Kim, H. Y., von Dassow, M., Zhang, L. and Zhou, J. (2010). Emergent morphogenesis: elastic mechanics of a self-deforming tissue. *J Biomech* **43**, 63-70.

Davidson, L. A., Marsden, M., Keller, R. and Desimone, D. W. (2006). Integrin alpha5beta1 and fibronectin regulate polarized cell protrusions required for Xenopus convergence and extension. *Curr Biol* **16**, 833-44.

Diz-Munoz, A., Krieg, M., Bergert, M., Ibarlucea-Benitez, I., Muller, D. J., Paluch, E. and Heisenberg, C. P. (2010). Control of directed cell migration in vivo by membrane-to-cortex attachment. *PLoS Biol* **8**, e1000544.

Diz-Munoz, A., Romanczuk, P., Yu, W., Bergert, M., Ivanovitch, K., Salbreux, G., Heisenberg, C. P. and Paluch, E. K. (2016). Steering cell migration by alternating blebs and actin-rich protrusions. *BMC Biol* **14**, 74.

Dohn, M. R., Mundell, N. A., Sawyer, L. M., Dunlap, J. A. and Jessen, J. R. (2013). Planar cell polarity proteins differentially regulate extracellular matrix organization and assembly during zebrafish gastrulation. *Dev Biol* **383**, 39-51.

Faix, J. and Rottner, K. (2006). The making of filopodia. *Curr Opin Cell Biol* **18**, 18-25.

Friedl, P. and Gilmour, D. (2009). Collective cell migration in morphogenesis, regeneration and cancer. *Nat Rev Mol Cell Biol* **10**, 445-57.

Gao, B., Song, H., Bishop, K., Elliot, G., Garrett, L., English, M. A., Andre, P., Robinson, J., Sood, R., Minami, Y. et al. (2011). Wnt signaling gradients

establish planar cell polarity by inducing Vangl2 phosphorylation through Ror2. *Dev Cell* **20**, 163-76.

Gilmour, D. T., Jessen, J.R., Lin, S. (2002). Manipulating gene expression in the zebrafish. In *Zebrafish, a practical approach*, vol. 261 (ed. C. Nusslein-Volhard, Dahm, R.), pp. 121-143. New York: Oxford University Press.

Goodrich, L. V. and Strutt, D. (2011). Principles of planar polarity in animal development. *Development* **138**, 1877-92.

Goto, T., Davidson, L., Asashima, M. and Keller, R. (2005). Planar cell polarity genes regulate polarized extracellular matrix deposition during frog gastrulation. *Curr Biol* **15**, 787-93.

Gray, R. S., Roszko, I. and Solnica-Krezel, L. (2011). Planar cell polarity: coordinating morphogenetic cell behaviors with embryonic polarity. *Dev Cell* **21**, 120-33.

Habas, R., Dawid, I. B. and He, X. (2003). Coactivation of Rac and Rho by Wnt/Frizzled signaling is required for vertebrate gastrulation. *Genes Dev* **17**, 295-309.

Habas, R., Kato, Y. and He, X. (2001). Wnt/Frizzled activation of Rho regulates vertebrate gastrulation and requires a novel Formin homology protein Daam1. *Cell* **107**, 843-54.

Heisenberg, C. P. and Nusslein-Volhard, C. (1997). The function of silberblick in the positioning of the eye anlage in the zebrafish embryo. *Dev Biol* **184**, 85-94.

Heisenberg, C. P., Tada, M., Rauch, G. J., Saude, L., Concha, M. L., Geisler, R., Stemple, D. L., Smith, J. C. and Wilson, S. W. (2000). Silberblick/Wnt11 mediates convergent extension movements during zebrafish gastrulation. *Nature* **405**, 76-81.

Jessen, J. R. and Solnica-Krezel, L. (2004). Identification and developmental expression pattern of van gogh-like 1, a second zebrafish strabismus homologue. *Gene Expr Patterns* **4**, 339-44.

Jessen, J. R. and Solnica-Krezel, L. (2005). Morphogenetic cell movements shaping the zebrafish gastrula. In *Planar cell polarization during development*, vol. 14 (ed. M. Mlodzik), pp. 131-165. San Diego: Elsevier Press.

Jessen, J. R., Topczewski, J., Bingham, S., Sepich, D. S., Marlow, F., Chandrasekhar, A. and Solnica-Krezel, L. (2002). Zebrafish trilobite identifies new roles for Strabismus in gastrulation and neuronal movements. *Nat Cell Biol* **4**, 610-5.

Jessen, T. N. and Jessen, J. R. (2017). VANGL2 interacts with integrin alphav to regulate matrix metalloproteinase activity and cell adhesion to the extracellular matrix. *Exp Cell Res* **361**, 265-276.

Julich, D., Geisler, R. and Holley, S. A. (2005). Integrinalpha5 and delta/notch signaling have complementary spatiotemporal requirements during zebrafish somitogenesis. *Dev Cell* **8**, 575-86.

Kilian, B., Mansukoski, H., Barbosa, F. C., Ulrich, F., Tada, M. and Heisenberg, C. P. (2003). The role of Ppt/Wnt5 in regulating cell shape and movement during zebrafish gastrulation. *Mech Dev* **120**, 467-76.

Kimmel, C. B., Ballard, W. W., Kimmel, S. R., Ullmann, B. and Schilling, T. F. (1995). Stages of embryonic development of the zebrafish. *Dev Dyn* **203**, 253-310.

Koshida, S., Kishimoto, Y., Ustumi, H., Shimizu, T., Furutani-Seiki, M., Kondoh, H. and Takada, S. (2005). Integrinalpha5-dependent fibronectin accumulation for maintenance of somite boundaries in zebrafish embryos. *Dev Cell* **8**, 587-98.

Latimer, A. and Jessen, J. R. (2010). Extracellular matrix assembly and organization during zebrafish gastrulation. *Matrix Biol* **29**, 89-96.

Lawrence, P. A. (1966). Development and determination of hairs and bristles in the milkweed bug, Oncopeltus fasciatus (Lygaeidae, Hemiptera). *J Cell Sci* **1**, 475-98.

Marlow, F., Topczewski, J., Sepich, D. and Solnica-Krezel, L. (2002). Zebrafish Rho kinase 2 acts downstream of Wnt11 to mediate cell polarity and effective convergence and extension movements. *Curr Biol* **12**, 876-84.

Marlow, F., Zwartkruis, F., Malicki, J., Neuhauss, S. C., Abbas, L., Weaver, M., Driever, W. and Solnica-Krezel, L. (1998). Functional interactions of genes mediating convergent extension, knypek and trilobite, during the partitioning of the eye primordium in zebrafish. *Dev Biol* **203**, 382-99.

Merte, J., Jensen, D., Wright, K., Sarsfield, S., Wang, Y., Schekman, R. and Ginty, D. D. (2009). Sec24b selectively sorts Vangl2 to regulate planar cell polarity during neural tube closure. *Nat Cell Biol* **12**, 41-6; sup pp 1-8.

Nubler-Jung, K., Bonitz, R. and Sonnenschein, M. (1987). Cell polarity during wound healing in an insect epidermis. *Development* **100**, 163-70.

Ohkawara, B., Yamamoto, T. S., Tada, M. and Ueno, N. (2003). Role of glypican 4 in the regulation of convergent extension movements during gastrulation in Xenopus laevis. *Development* **130**, 2129-38.

Parsons, M. J., Pollard, S. M., Saude, L., Feldman, B., Coutinho, P., Hirst, E. M. and Stemple, D. L. (2002). Zebrafish mutants identify an essential role for laminins in notochord formation. *Development* **129**, 3137-46.

Riedl, J., Crevenna, A. H., Kessenbrock, K., Yu, J. H., Neukirchen, D., Bista, M., Bradke, F., Jenne, D., Holak, T. A., Werb, Z. et al. (2008). Lifeact: a versatile marker to visualize F-actin. *Nat Methods* **5**, 605-7.

Roszko, I., Sawada, A. and Solnica-Krezel, L. (2009). Regulation of convergence and extension movements during vertebrate gastrulation by the Wnt/PCP pathway. *Semin Cell Dev Biol* **20**, 986-97.

Roszko, I., Sepich, D. S., Jessen, J. R., Chandrasekhar, A. and Solnica-Krezel, L. (2015). A dynamic intracellular distribution of Vangl2 accompanies cell polarization during zebrafish gastrulation. *Development* **142**, 2508-20.

Schindelin, J., Arganda-Carreras, I., Frise, E., Kaynig, V., Longair, M., Pietzsch, T., Preibisch, S., Rueden, C., Saalfeld, S., Schmid, B. et al. (2012). Fiji: an open-source platform for biological-image analysis. *Nat Methods* **9**, 676-82.

Schwarzbauer, J. E. and DeSimone, D. W. (2011). Fibronectins, their fibrillogenesis, and in vivo functions. *Cold Spring Harb Perspect Biol* **3**.

Sedzinski, J., Biro, M., Oswald, A., Tinevez, J. Y., Salbreux, G. and Paluch, E. (2011). Polar actomyosin contractility destabilizes the position of the cytokinetic furrow. *Nature* **476**, 462-6.

Seo, H. S., Habas, R., Chang, C. and Wang, J. (2017). Bimodal regulation of Dishevelled function by Vangl2 during morphogenesis. *Hum Mol Genet* **26**, 2053-2061.

Sepich, D. S., Calmelet, C., Kiskowski, M. and Solnica-Krezel, L. (2005). Initiation of convergence and extension movements of lateral mesoderm during zebrafish gastrulation. *Dev Dyn* **234**, 279-92.

Sepich, D. S., Myers, D. C., Short, R., Topczewski, J., Marlow, F. and Solnica-Krezel, L. (2000). Role of the zebrafish trilobite locus in gastrulation movements of convergence and extension. *Genesis* **27**, 159-73.

Solnica-Krezel, L., Schier, A. F. and Driever, W. (1994). Efficient recovery of ENU-induced mutations from the zebrafish germline. *Genetics* **136**, 1401-20.

Solnica-Krezel, L., Stemple, D. L., Mountcastle-Shah, E., Rangini, Z., Neuhauss, S. C., Malicki, J., Schier, A. F., Stainier, D. Y., Zwartkruis, F., Abdelilah, S. et al. (1996). Mutations affecting cell fates and cellular rearrangements during gastrulation in zebrafish. *Development* **123**, 67-80.

Strutt, D. and Strutt, H. (2007). Differential activities of the core planar polarity proteins during Drosophila wing patterning. *Dev Biol* **302**, 181-94.

Strutt, D. I. (2002). The asymmetric subcellular localisation of components of the planar polarity pathway. *Semin Cell Dev Biol* **13**, 225-31.

Strutt, H. and Strutt, D. (2009). Asymmetric localisation of planar polarity proteins: Mechanisms and consequences. *Semin Cell Dev Biol* **20**, 957-63.

Sun, L., Zou, Z., Collodi, P., Xu, F., Xu, X. and Zhao, Q. (2005). Identification and characterization of a second fibronectin gene in zebrafish. *Matrix Biol* **24**, 69-77.

Taylor, J., Abramova, N., Charlton, J. and Adler, P. N. (1998). Van Gogh: a new Drosophila tissue polarity gene. *Genetics* **150**, 199-210.

Thisse, B., Pflumio, S., Furthauer, M., Loppin, B. Heyer, V., Degrave, A., Woehl, R. Lux, A., Steffan, T., Charbonnier, X.Q., Thisse, C. (2001). Expression of the zebrafish genome during embryogenesis. ZFIN direct data submission (http://zfin.org).

Thisse, C. and Thisse, B. (2008). High-resolution in situ hybridization to whole-mount zebrafish embryos. *Nat Protoc* **3**, 59-69.

Topczewski, J., Sepich, D. S., Myers, D. C., Walker, C., Amores, A., Lele, Z., Hammerschmidt, M., Postlethwait, J. and Solnica-Krezel, L. (2001). The zebrafish glypican knypek controls cell polarity during gastrulation movements of convergent extension. *Dev Cell* **1**, 251-64.

Trinh, L. A. and Stainier, D. Y. (2004). Fibronectin regulates epithelial organization during myocardial migration in zebrafish. *Dev Cell* **6**, 371-82.

Veeman, M. T., Slusarski, D. C., Kaykas, A., Louie, S. H. and Moon, R. T. (2003). Zebrafish prickle, a modulator of noncanonical Wnt/Fz signaling, regulates gastrulation movements. *Curr Biol* **13**, 680-5.

Westerfield, M. (2000). The zebrafish book. A guide for the laboratory use of zebrafish (Danio rerio). Eugene: University of Oregon Press.

Williams, B. B., Cantrell, V. A., Mundell, N. A., Bennett, A. C., Quick, R. E. and Jessen, J. R. (2012). VANGL2 regulates membrane trafficking of MMP14 to control cell polarity and migration. *J Cell Sci* **125**, 2141-2147.

Winklbauer, R. and Keller, R. E. (1996). Fibronectin, mesoderm migration, and gastrulation in Xenopus. *Dev Biol* **177**, 413-26.

Wong, L. L. and Adler, P. N. (1993). Tissue polarity genes of Drosophila regulate the subcellular location for prehair initiation in pupal wing cells. *J Cell Biol* **123**, 209-21.

Wu, J. and Mlodzik, M. (2009). A quest for the mechanism regulating global planar cell polarity of tissues. *Trends Cell Biol*.

Yang, Y. and Mlodzik, M. (2015). Wnt-Frizzled/planar cell polarity signaling: cellular orientation by facing the wind (Wnt). *Annu Rev Cell Dev Biol* **31**, 623-46.

Yin, C., Ciruna, B. and Solnica-Krezel, L. (2009). Convergence and extension movements during vertebrate gastrulation. *Curr Top Dev Biol* **89**, 163-92.

Yin, C., Kiskowski, M., Pouille, P. A., Farge, E. and Solnica-Krezel, L. (2008). Cooperation of polarized cell intercalations drives convergence and extension of presomitic mesoderm during zebrafish gastrulation. *J Cell Biol* **180**, 221-32.

Figures

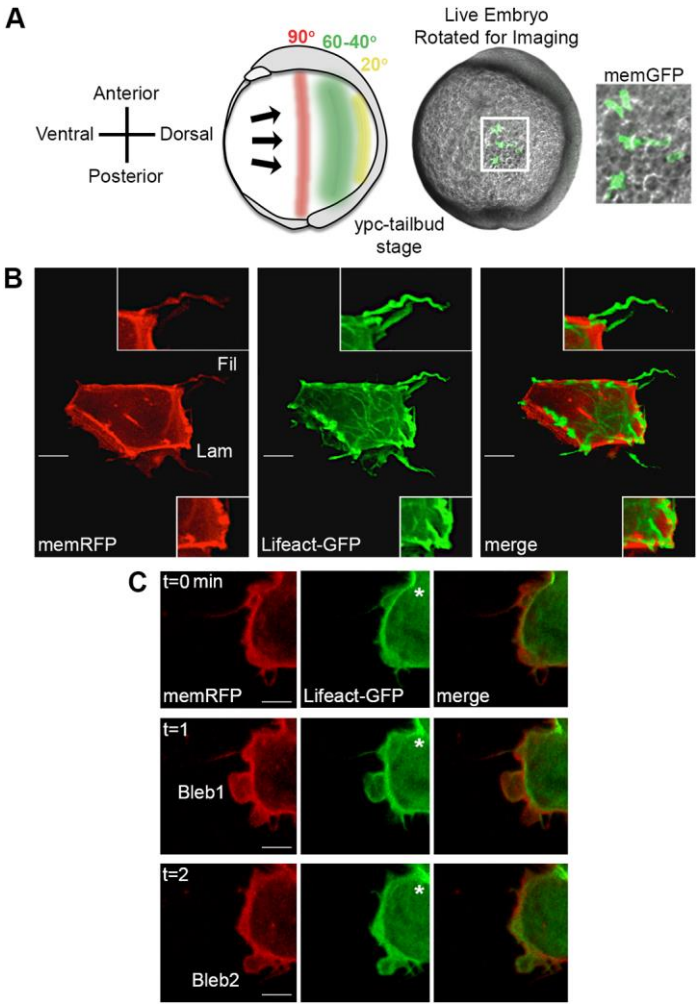

Fig. 1. Time-lapse imaging of membrane protrusions. (A) Schematic representation and live wild-type zebrafish embryo highlighting the 40°-60° lateral region analyzed. Lateral ectodermal cells with mosaic memGFP expression from an embryo used for confocal imaging at 60° from dorsal (white box area enlarged). ypc, yolk-plug closure. (B) Wild-type ectodermal cell expressing memRFP and Lifeact-GFP with filopodia (Fil) and large lamellipodia-like (Lam) membrane protrusions. White boxed areas include enlarged images of protrusion classifications. (C) Wild-type ectodermal cell undergoing division. Asterisks indicate forming cleavage furrow. Two blebs are observed during the three time points. Scale bars, 5 μm.

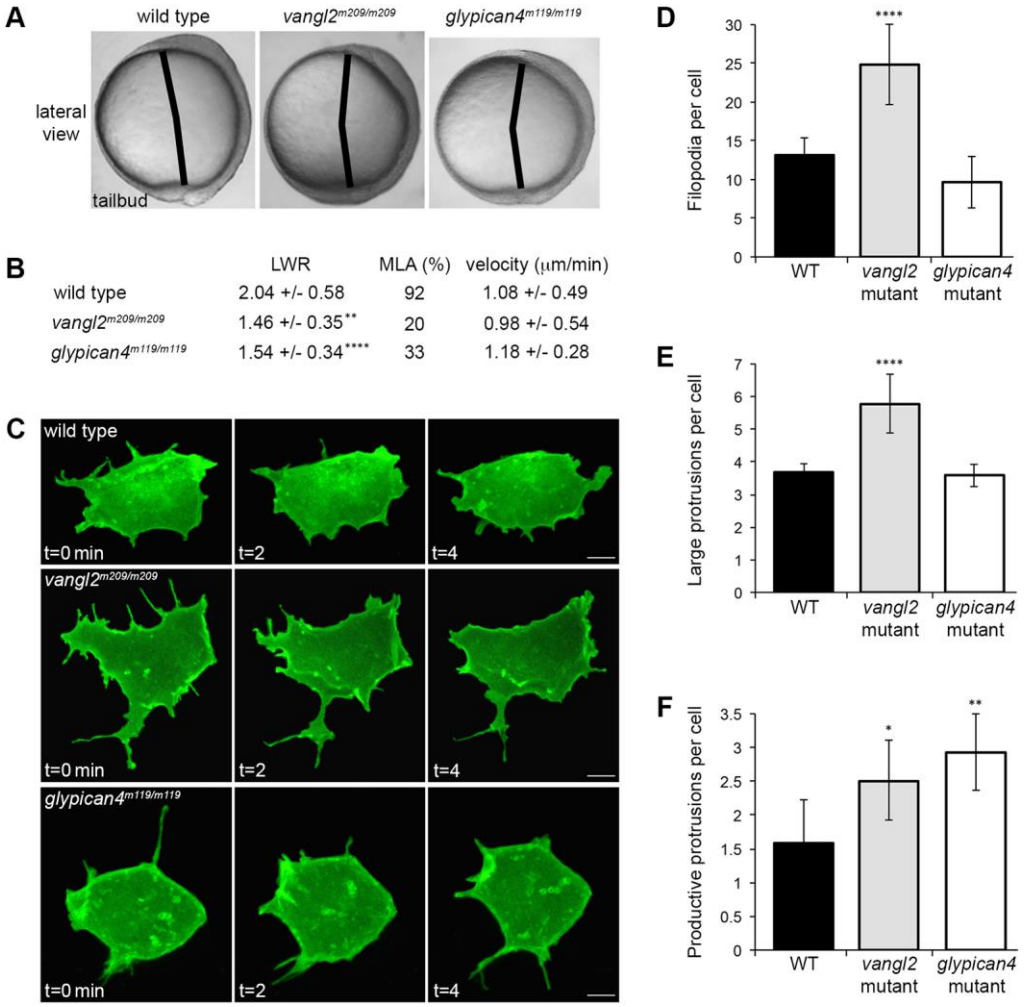

Fig. 2. Membrane protrusion formation in *vangl2* and *glypican4* mutant embryos. (A) Live embryo images at late yolk-plug closure/tailbud stage. Black lines denote the polster-tailbud angle. (B) PCP and migration velocity quantitation in the ectoderm. LWR and MLA values were obtained from: wild type (WT) n=50 cells, 13 embryos; *vangl2*$^{m209/m209}$ n=10 cells, 8 embryos; *glypican4*$^{m119/m119}$ n=49 cells, 5 embryos. PCP data for *vangl2* mutant ectoderm was previously published (Jessen et al., 2002), thus the lower n. (C) Time-lapse confocal images of ectodermal cells expressing memGFP over three time points. (D-F) Quantitation of the total numbers of protrusions and productive protrusions formed by wild type (n=12 cells, 8 embryos), *vangl2*$^{m209/m209}$ (n=10 cells, 7 embryos), and *glypican4*$^{m119/m119}$ (n=12 cells, 5 embryos). Average values are shown ± standard deviation. **P*<0.05, ***P*<0.01, ****P*<0.001, *****P*<0.0001; *P* values are versus wild type; one-way ANOVA significance test followed by Tukey HSD post-hoc tests. Scale bars, 5 μm.

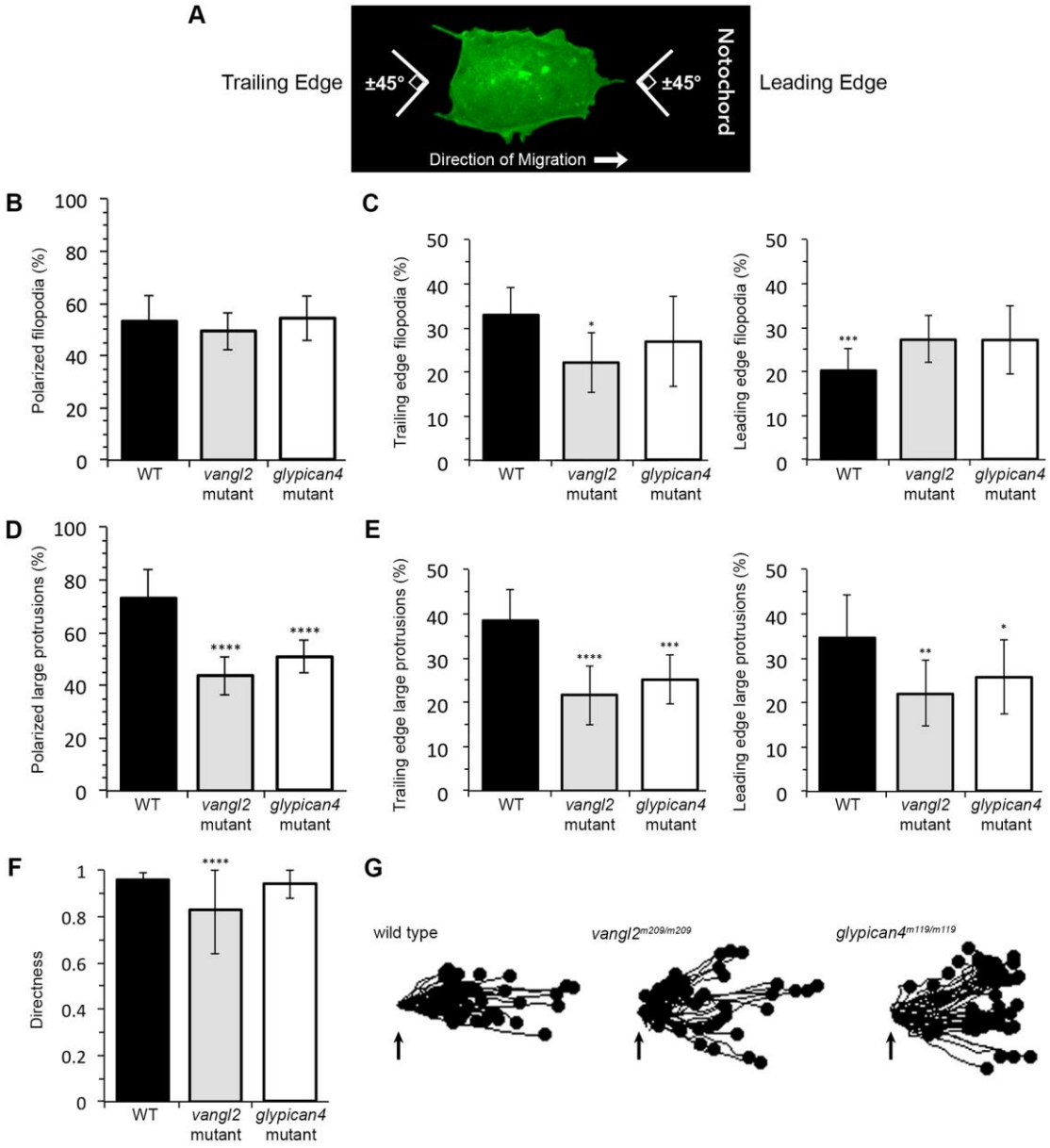

Fig. 3. Membrane protrusion polarity and directed migration in *vangl2* and *glypican4* mutant embryos. (A) Wild-type (WT) ectodermal cell image illustrating polarized protrusion angles. (B,C) Quantitation of the total percentages of polarized filopodia and filopodia localized at the leading versus trailing edge in wild type (n=11 cells, 8 embryos), *vangl2*$^{m209/m209}$ (n=10 cells, 7 embryos), and *glypican4*$^{m119/m119}$ (n=11 cells, 5 embryos). (D,E) Similar to filopodia analysis in (B,C), quantitation of large protrusions (WT n=12 cells, 8 embryos; *vangl2*$^{m209/m209}$ n=10 cells, 7 embryos; *glypican4*$^{m119/m119}$ n=12 cells, 5 embryos). (F) Directed migration values (WT n=50 cells, 11 embryos; *vangl2*$^{m209/m209}$ n=51 cells, 13 embryos; *glypican4*$^{m119/m119}$ n=50 cells, 8 embryos). (G) Schematic representations of the migration paths of individual ectodermal

cells. Origins (arrows) standardized for comparison. Dorsal is to the right. Average values are shown ± standard deviation. *P<0.05, **P<0.01, ***P<0.001, ****P<0.0001; P values are versus wild type, except WT leading edge P value is versus WT trailing edge; one-way ANOVA significance test followed by Tukey HSD post-hoc tests.

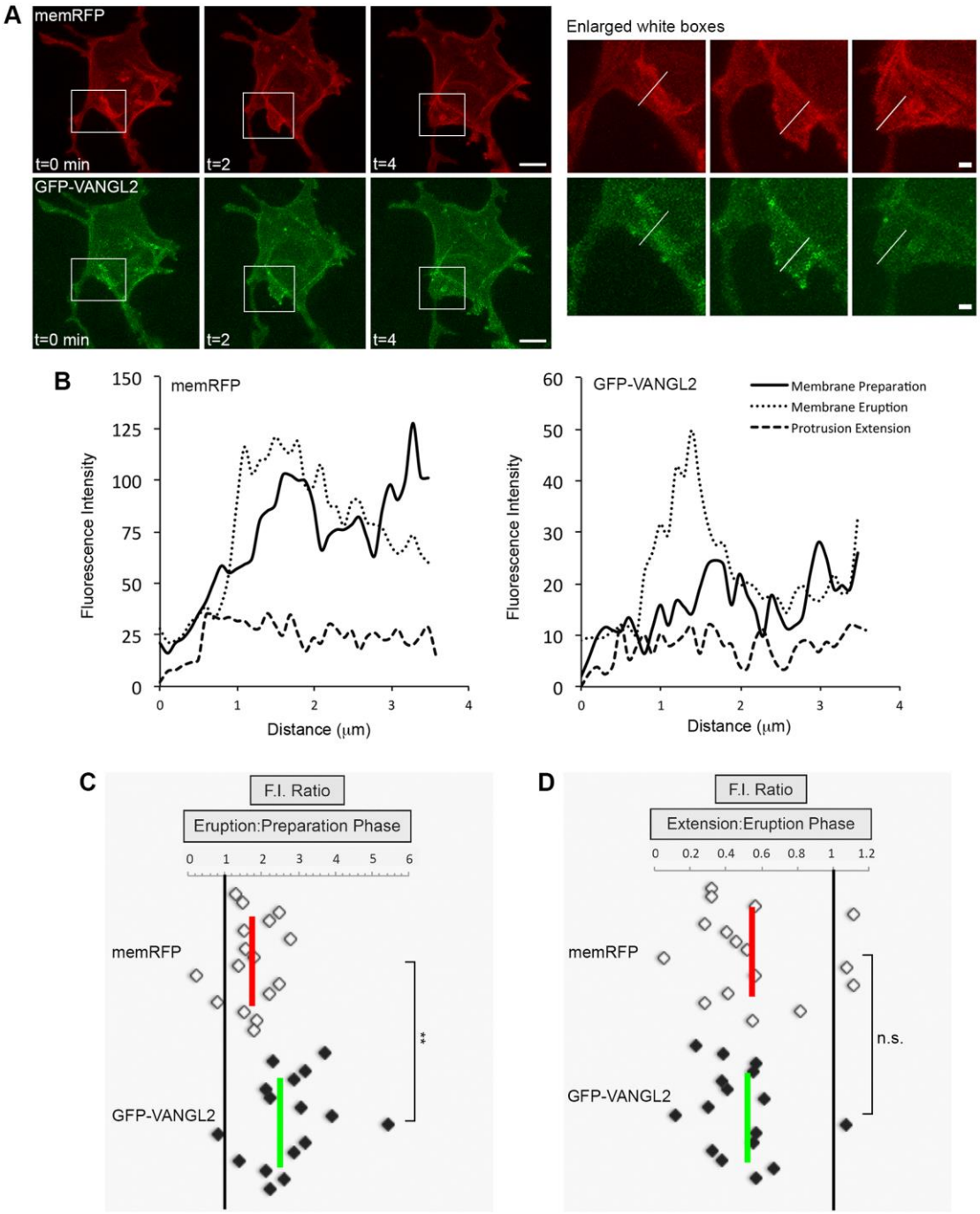

Fig. 4. Increased Vangl2 expression in forming membrane protrusions. (A) Time-lapse confocal images of wild-type lateral ectodermal cells expressing memRFP and GFP-VANGL2 (three time points shown). White boxes highlight a forming large protrusion (enlarged images on the right; white lines approximate the regions analyzed). (B) Plot profiles of fluorescence intensity (F.I.) across the plasma membrane of an

individual large protrusion expressing memRFP and GFP-VANGL2 prior to protrusion formation (preparation), after formation (eruption), and during extension. (C,D) memRFP and GFP-VANGL2 F.I. ratios for individual large protrusions (eruption phase/preparation phase n=16 protrusions, 6 embryos; extension phase/eruption phase n=16 protrusions, 6 embryos). Vertical red and green lines indicate the averages. $^{**}P<0.01$, n.s. not significant; two-tailed paired *t*-test. Scale bars, 5 μm (A, left) and 1 μm (A, right).

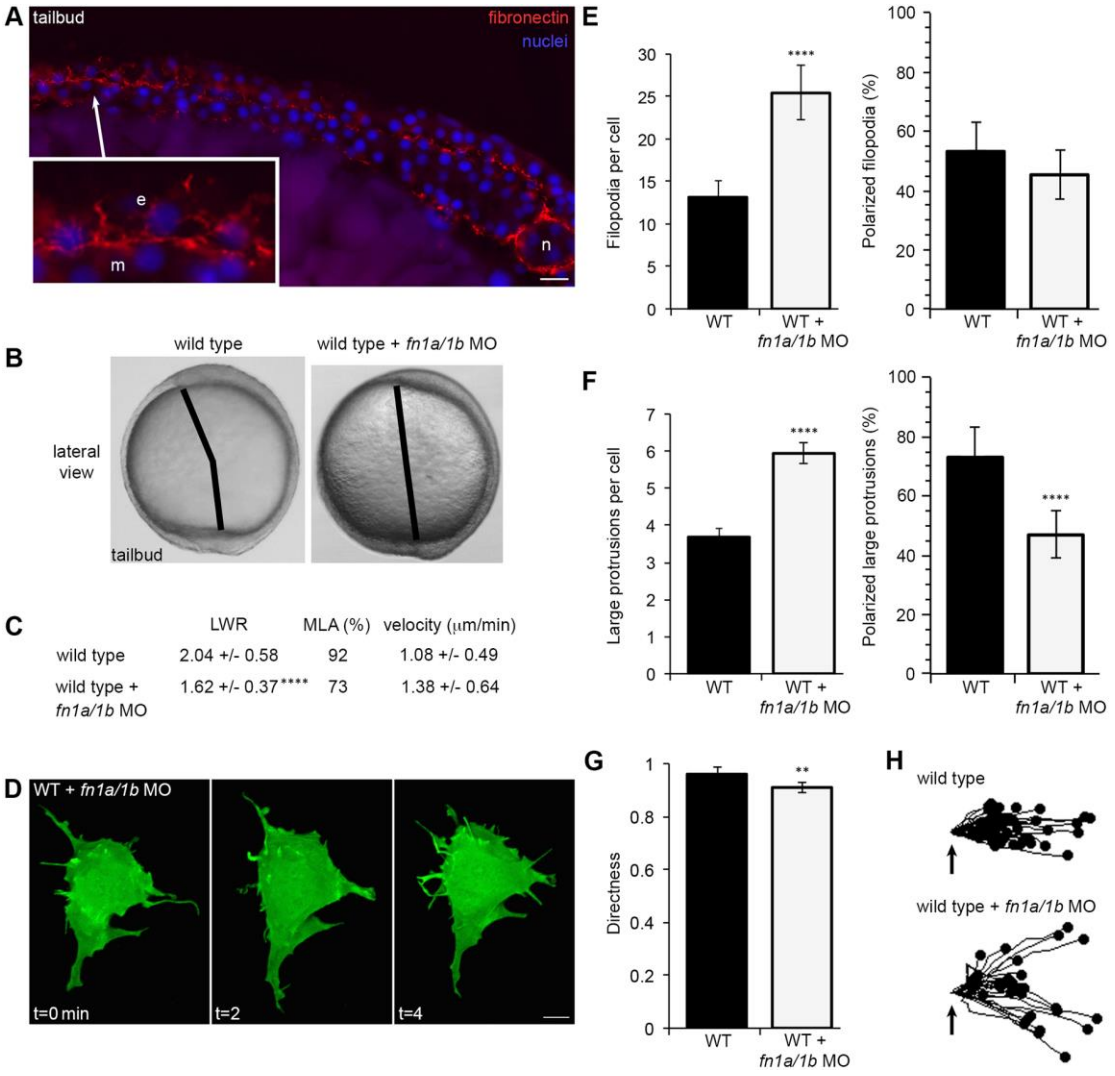

Fig. 5. Fibronectin regulates membrane protrusion dynamics. (A) Cryosection through the dorsolateral region of a wild-type (WT) tailbud stage embryo showing fibronectin and nuclei. The white box is an enlarged image illustrating the relationship between ECM and ectodermal (e) and mesodermal (m) cells. n, notochord. (B) Live embryo images at late yolk-plug closure/tailbud stage. Black lines denote the polster-tailbud angle. (C) PCP and migration velocity quantitation of ectodermal cells. LWR and MLA values were obtained from: wild type n values are as in Fig. 2; *fn1a/1b* morpholino (MO)-injected wild type n=48 cells, 10 embryos. (D) Representative ectodermal cell expressing memGFP over three time points from time-lapse data. (E,F) Quantitation of the average total number of protrusions and the total percentage of polarized protrusions in wild type (n values are as in Figs 2 and 3) and *fn1a/1b* morphant embryos (n=10 cells, 7 embryos). (G) Directed migration values (wild type n values are as in Fig. 3; *fn1a/1b*

morphants n=32 cells, 10 embryos). (H) Schematic representations of the migration paths of individual ectodermal cells. Origins (arrows) standardized for comparison. Dorsal is to the right. Average values are shown ± standard deviation. $^{**}P<0.01$, $^{****}P<0.0001$; *P* values are versus wild type; two-tailed unpaired *t*-test. Scale bars: 20 μm in panel A; 5 μm panel D.

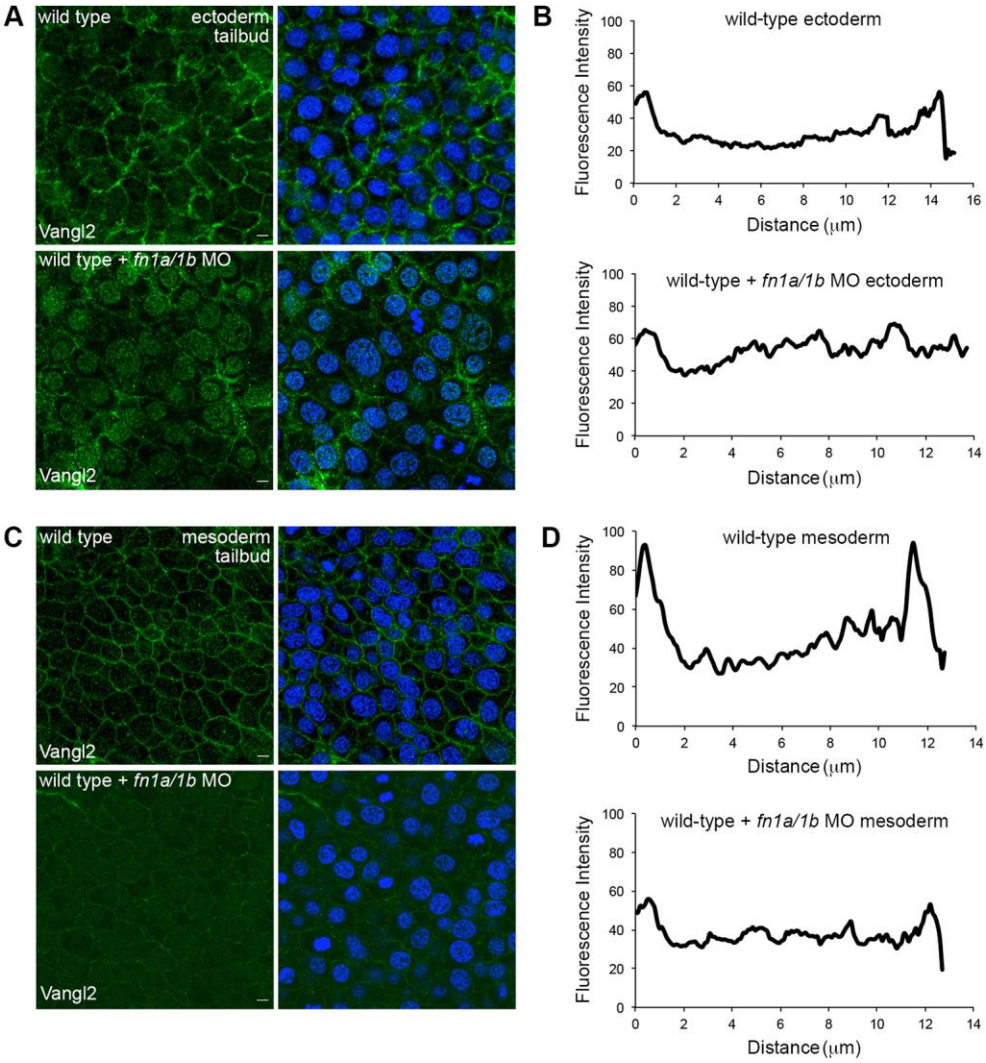

Fig. 6. Fibronectin is required for cell surface Vangl2 expression. (A,C) Zebrafish Vangl2 protein expression in wild type and *fn1a/1b* morpholino (MO)-injected tailbud stage embryos without (left panels) and with (right panels) DAPI nuclear labeling. Immunofluorescence labeling of Vangl2 in the ectoderm (A) and mesoderm (C). (B,D) Representative plot profiles showing average fluorescence intensities across single ectodermal cells in wild type (n=30 cells, 3 embryos) and *fn1a/1b* morphant embryos (n=30 cells, 3 embryos). (B) ectoderm. (D) mesoderm. Scale bars, 5 μm.

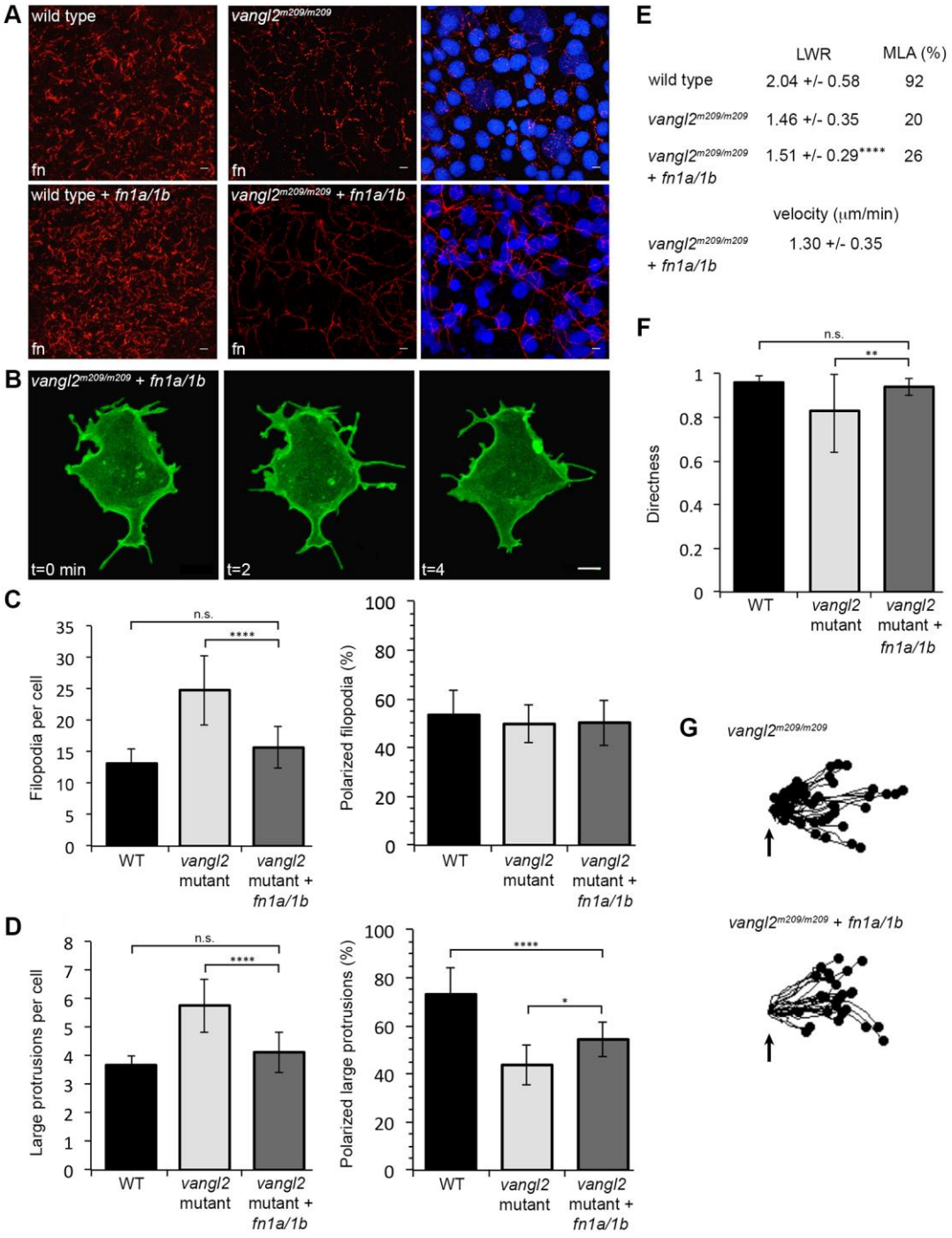

Fig. 7. Fibronectin expression rescues the *vangl2* membrane protrusion phenotype but not PCP. (A) Fibronectin expression in tailbud stage wild type (WT) and *vangl2*$^{m209/m209}$ mutant control embryos (top images) or wild type and mutant embryos injected with *fn1a/1b* synthetic mRNA (bottom images). Nuclei labeled with DAPI (right images). fn, fibronectin. (B) Representative ectodermal cell expressing memGFP over

three points from time-lapse data. (C,D) Quantitation of the average total number of protrusions and the total percentage of polarized protrusions in *vangl2*$^{m209/m209}$ mutant control embryos (n values are as in Figs 2 and 3) and *vangl2*$^{m209/m209}$ mutants injected with *fn1a/1b* mRNA (n=10 cells, 7 embryos). (E) PCP quantitation in the ectoderm. LWR and MLA values obtained from: *vangl2*$^{m209/m209}$ n values are as in Fig. 2; *fn1a/*1b-injected *vangl2*$^{m209/m209}$ mutants n=50 cells, 8 embryos. (F) Directed migration values (*vangl2*$^{m209/m209}$ n values are as in Fig. 3; *fn1a/1b*-injected *vangl2*$^{m209/m209}$ mutants n=26 cells, 8 embryos). (G) Schematic representations of the migration paths of individual ectodermal cells. Origins (arrows) standardized for comparison. Dorsal is to the right. Average values are shown ± standard deviation. **P*<0.05, ***P*<0.01, *****P*<0.0001, n.s. not significant; *P* values are versus wild type, except as indicated on the graphs; one-way ANOVA significance test followed by Tukey HSD post-hoc tests. Scale bars, 5 μm.

Fig. S1. Rose diagrams showing large membrane protrusion directionality around the cell circumference. Diagrams depicting the circular frequency and distribution of ectodermal cell large protrusions are shown for each experimental condition: wild type, *vangl2*$^{m209/m209}$ mutant embryos, *glypican4*$^{m119/m119}$ mutant embryos, *vangl2* mRNA injected wild-type embryos, *prickle1a* morpholino (MO) injected wild-type embryos, *fn1a/1b* MO injected embryos, and *fn1a/1b* mRNA injected *vangl2*$^{m209/m209}$ mutant embryos. The horizontal plane represents 0° and a mediolateral protrusion orientation while the vertical plane represents 90° and a anterior-posterior protrusion orientation. The position of the dorsal embryonic axis is indicated.

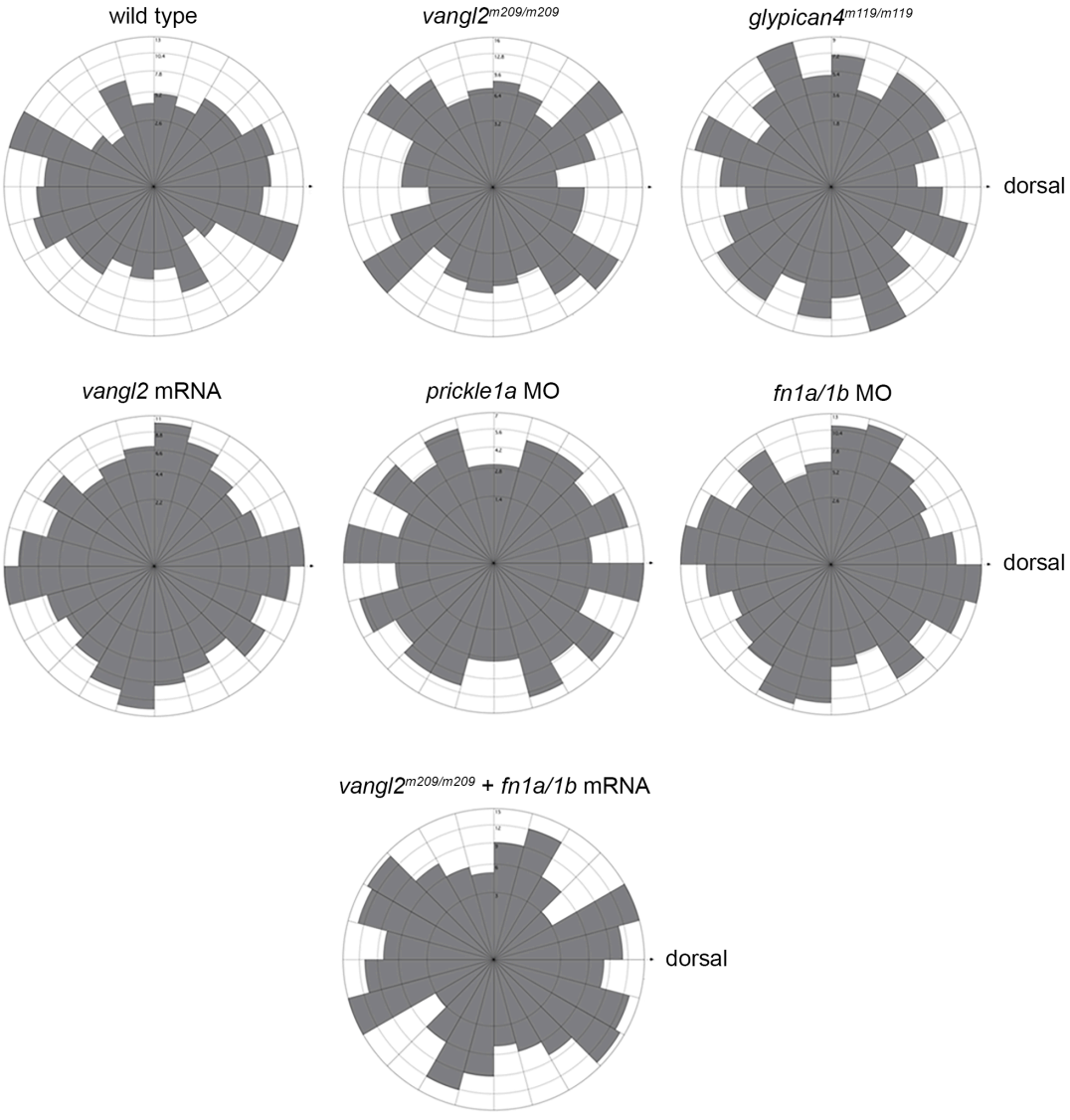

Fig. S2. Zebrafish Vangl2 polyclonal antibody validation and Vangl2 overexpression. (A) Immunofluorescence labeling of endogenous Vangl2 protein expression in wild-type (WT) tailbud stage embryo (right panel, nuclei labeled with DAPI). (B) Vangl2 expression in a wild-type embryo injected with 200 pg synthetic *vangl2* mRNA (right panel, nuclei labeled with DAPI). (C) Endogenous Vangl2 expression in a tailbud stage *vangl2*$^{vu7/vu7}$ mutant embryo. Only background fluorescence from the secondary antibody is visible. Scale bars: 5 μm in panels A and B; 20 μm panel C.

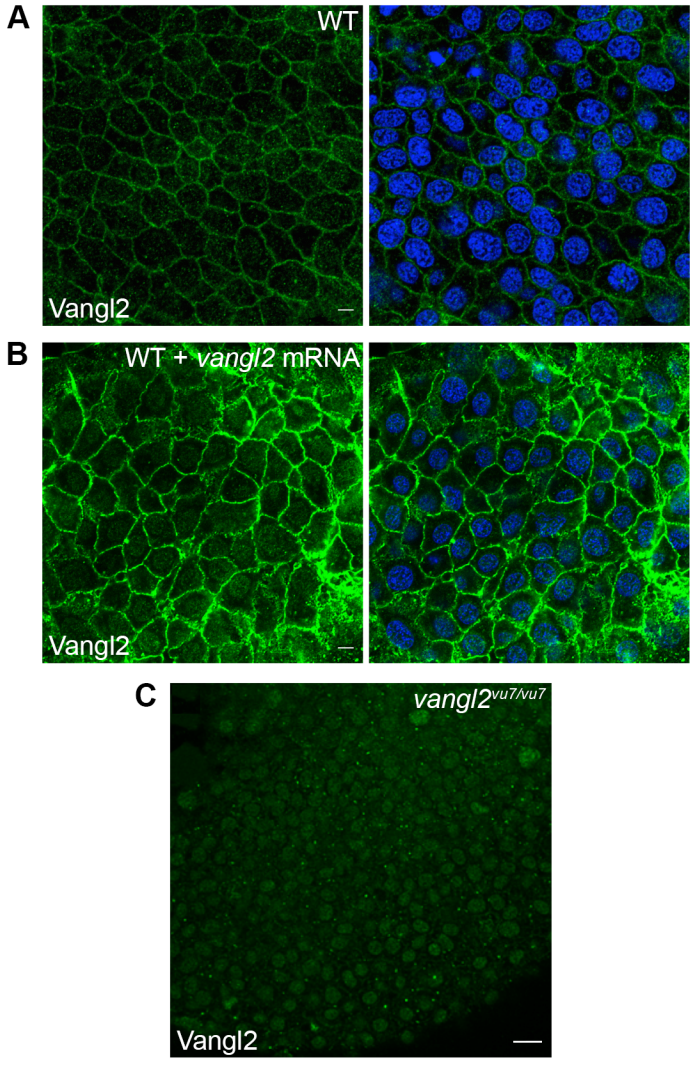

Fig. S3. Vangl2 overexpression disrupts PCP and membrane protrusion dynamics. (A) Western blot of Vangl2 protein expression in *vangl2* mRNA-injected wild-type (WT) embryos. Raw unmodified densitometry values are shown. (B) Upper panels, live images of late yolk-plug closure/tailbud stage embryos. Black lines denote the polster-tailbud angle. Lower panels, whole-mount *in situ* hybridizations performed using antisense RNA probes labeling the neural/non-neural ectoderm boundary (*dlx3b*), midline (*shha*), and prechordal mesendoderm (*ctslb*). (C) PCP and migration velocity quantitation in the ectoderm. LWR and MLA values were obtained from: wild type n values are as in Fig. 2; *vangl2*-injected wild type n=50 cells, 9 embryos. (D) Representative ectodermal cell expressing memGFP over three time points from time-lapse data. (E,F) Quantitation of the average total number of protrusions and the total percentage of polarized protrusions in wild type (n values are as in Figs 2 and 3) and *vangl2*-injected wild-type embryos (n=10 cells, 7 embryos). (G) Directed migration values (wild type n values are as in Fig. 3; *vangl2*-injected n=43 cells, 9 embryos). (H) Schematic representations of the migration paths of individual ectodermal cells. Origins (arrows) standardized for comparison. Dorsal is to the right. Average values are shown ± standard deviation. $^{**}P<0.01$, $^{****}P<0.0001$; *P* values are versus wild type; two-tailed unpaired *t*-test. Scale bar, 5 μm.

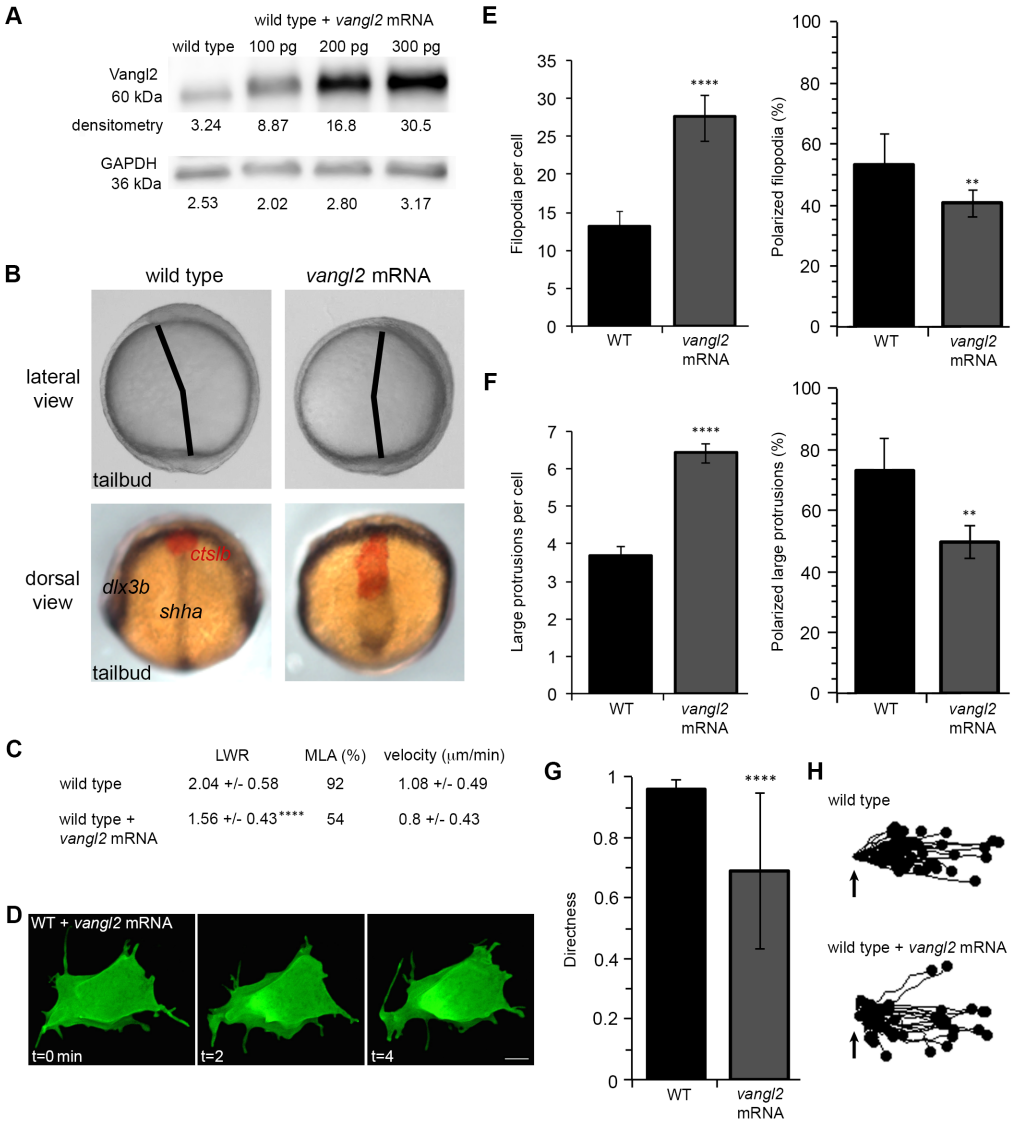

Figure S3

Fig. S4. Vangl2 expression in polarized migrating gastrula cells. (A) Tailbud-1-somite stage wild-type lateral ectodermal cells injected with memRFP and GFP-VANGL2 synthetic mRNA. (B,D) Plot profiles of fluorescence intensity (F.I.) across the anterior/posterior (B) and leading edge/trailing edge (D) axes of single ectodermal cells. (C,E) memRFP and GFP-VANGL2 anterior/posterior (C) and leading edge/trailing edge (E) membrane F.I. ratios for individual lateral ectodermal cells (anterior/posterior n=18 cells, 15 embryos; leading edge/trailing edge n=20 cells, 15 embryos). Horizontal and vertical red and green lines indicate averages. n.s. not significant; two-tailed paired *t*-test. Scale bars, 5 μm.

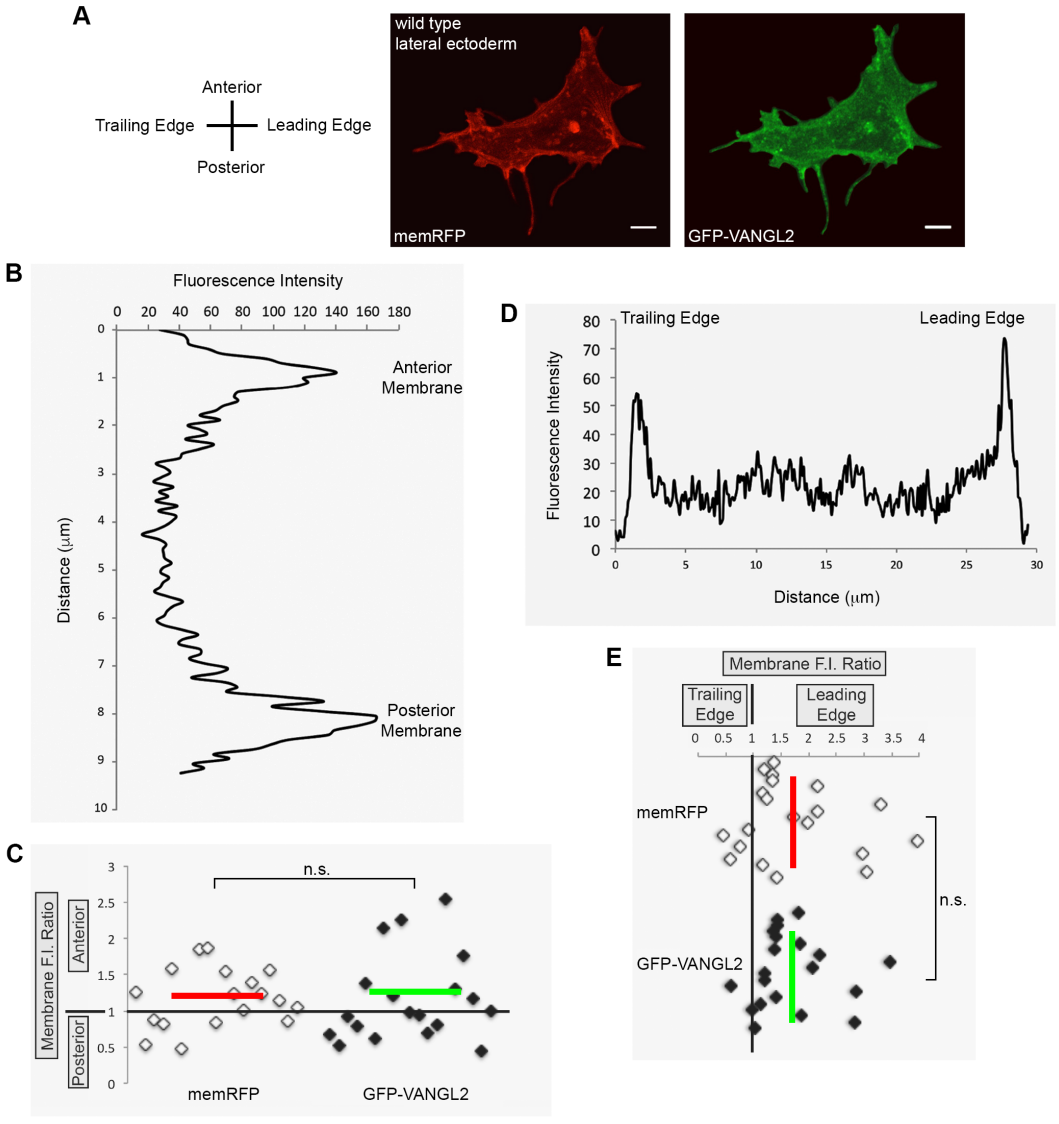

Fig. S5. GFP-VANGL2 localization in protrusive and non-protrusive membrane domains. (A) Lateral ectodermal cell labeled with memRFP and GFP-VANGL2. Arrows denote a forming non-polarized large protrusion. Arrowheads show a non-protrusive membrane domain. memRFP and GFP-VANGL2 fluorescence intensity (F.I.) ratios for (B) protrusive/non-protrusive membrane domains (n=9 protrusions, 6 embryos) and (C) polarized/non-polarized large protrusions (n=14 protrusions, 5 embryos). Vertical red and green lines indicate the averages. *P<0.05, n.s. not significant; two-tailed paired t-test. Scale bars, 5 μm.

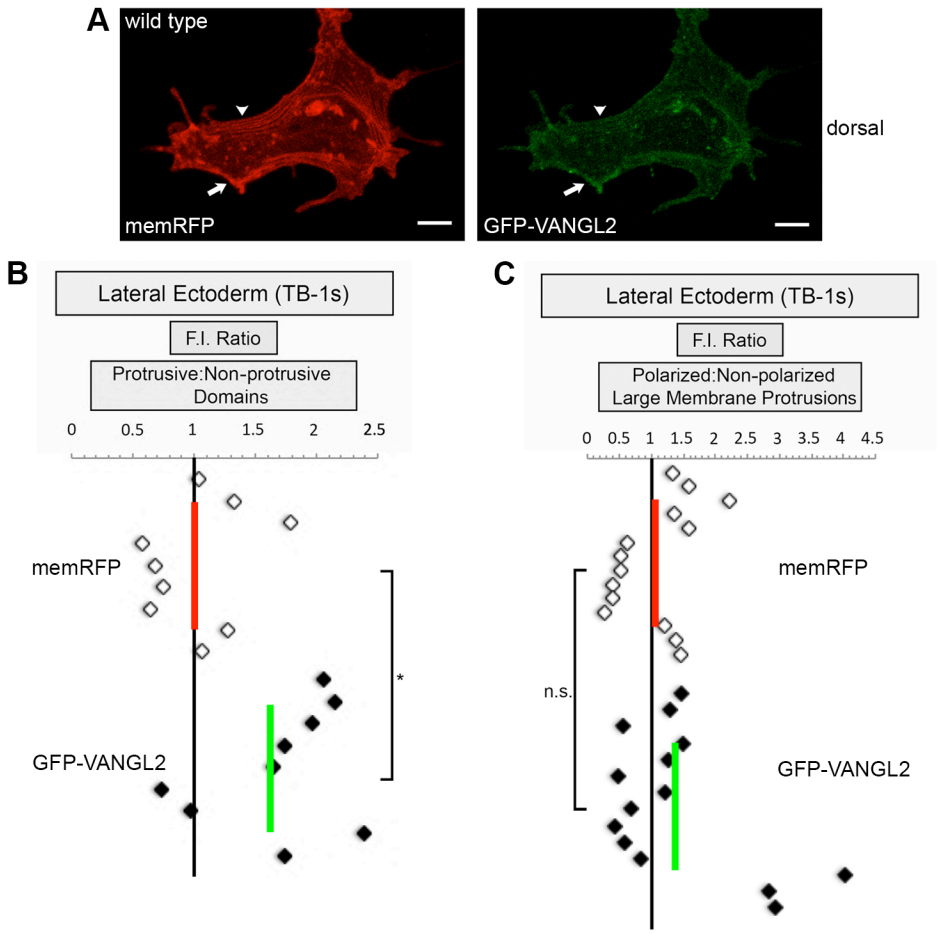

Fig. S6. Morpholino knockdown disrupts fibronectin expression and fibrillogenesis. (A) Immunofluorescence labeling of fibronectin expression in tailbud stage wild-type embryo and wild-type embryos injected with either 5 ng or 10 ng of each *fibronectin* morpholino (MO). (B) Injection of *fn1a/1b* synthetic mRNA rescues the *fn1a/1b* morpholino ECM phenotype. Bottom images in (A) and (B) show DAPI-labeled nuclei. Scale bars, 5 µm.

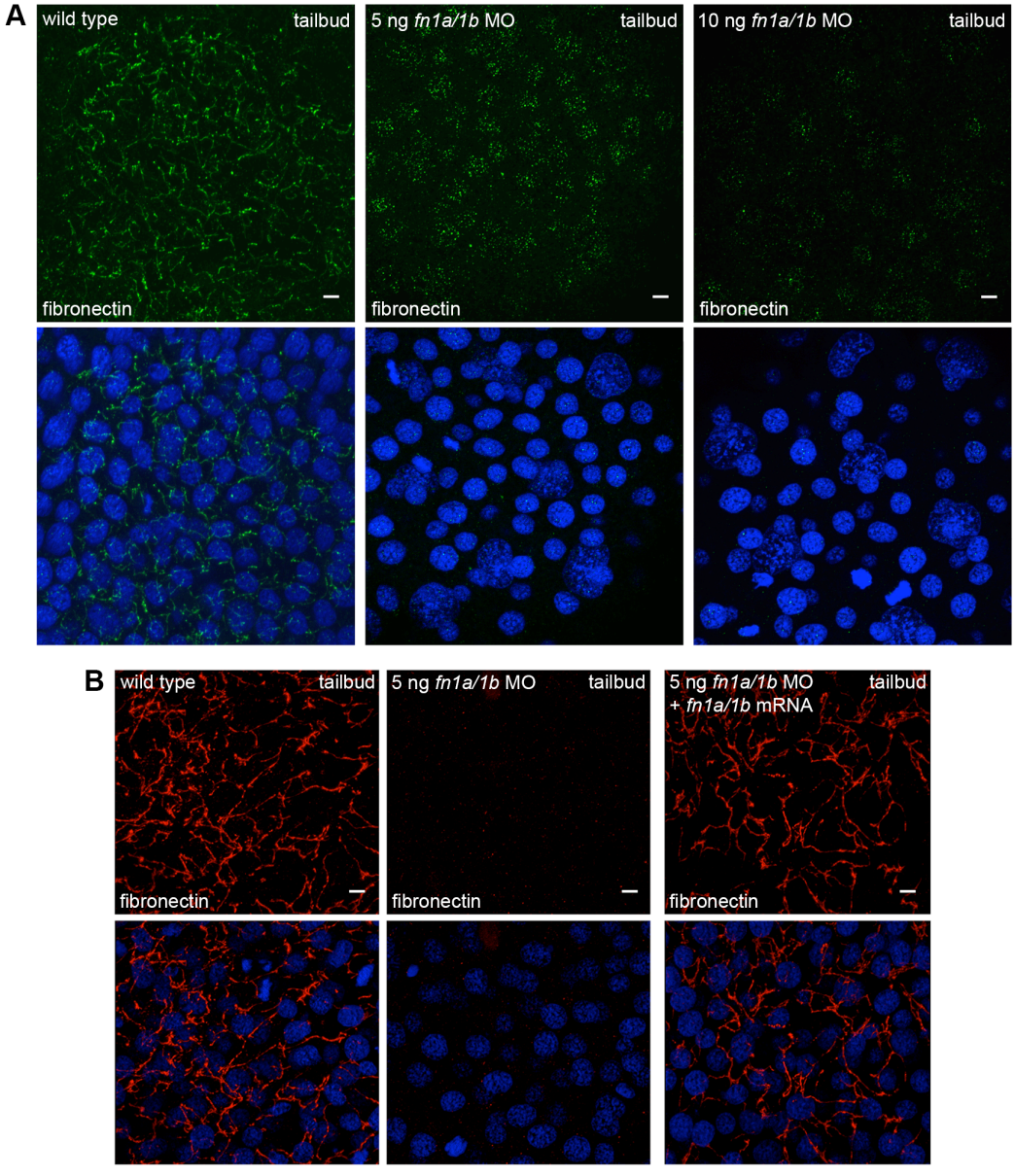

Fig. S7. Wild type and *vangl2* morphant membrane protrusive activity at mid-gastrulation. (A) Time-lapse confocal images of 80% epiboly epiblast cells expressing memGFP. WT, wild type. (B,C) Quantitation of the total numbers of membrane protrusions formed by wild type (n=9 cells, 7 embryos) and wild-type embryos injected with *vangl2* morpholino (MO) (n=10 cells, 6 embryos). (D) Quantitation of the total percentage of polarized large protrusions. Average values are shown ± standard deviation. ***P*<0.01; *P* values are versus wild type; two-tailed unpaired *t*-test. Scale bars, 5 µm.

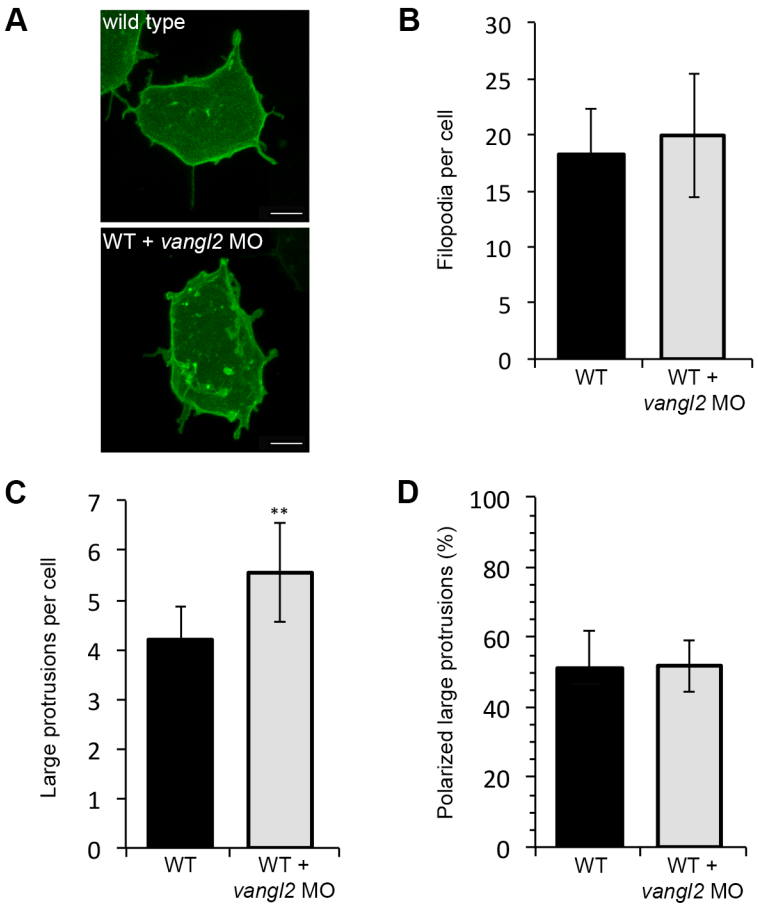

Fig. S8. Fibronectin is not required for Vangl2 expression at 60% epiboly. (A) Immunofluorescence labeling of Vangl2 protein expression in wild type and *fn1a/1b* morpholino (MO)-injected wild-type embryos without (left panels) and with (right panels) DAPI nuclear labeling. (B) Representative plot profiles showing the average fluorescence intensities across single epiblast cells in wild type (n=30 cells, 3 embryos) and *fn1a/1b* morphant embryos (n=30 cells, 3 embryos). Scale bars, 5 μm.

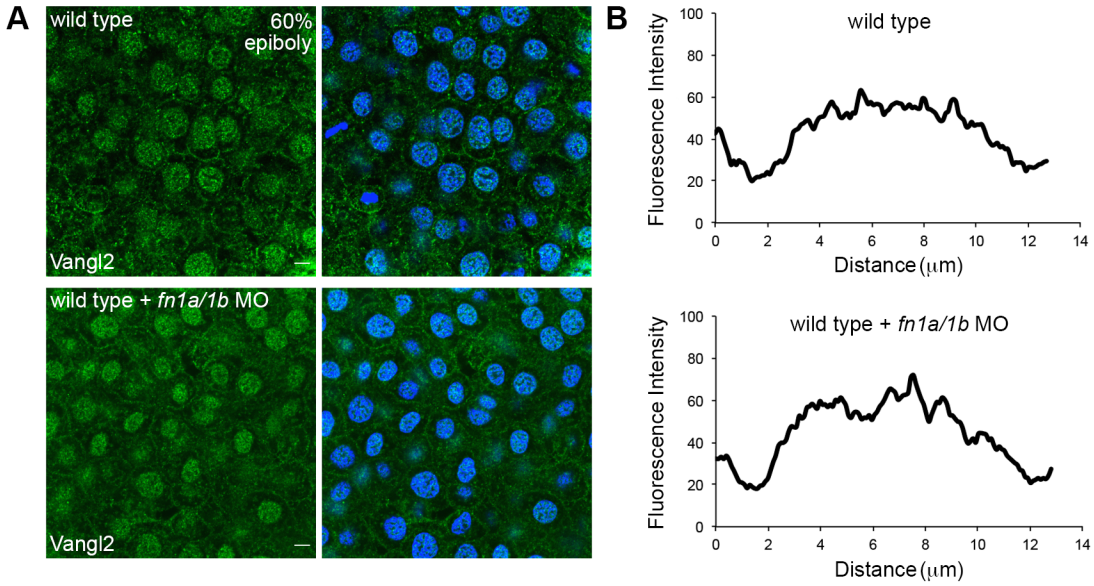

Fig. S9. Western blot analysis of Vangl2 expression in *fibronectin* morphants. Blots of total protein extracts from wild-type control embryos and wild-type embryos injected with 3, 6, 5, and 10 ng of each *fibronectin* morpholino (MO). Vangl2 labeled with a rabbit polyclonal antibody and actin loading control. Densitometry numbers for Vangl2 are normalized to actin.

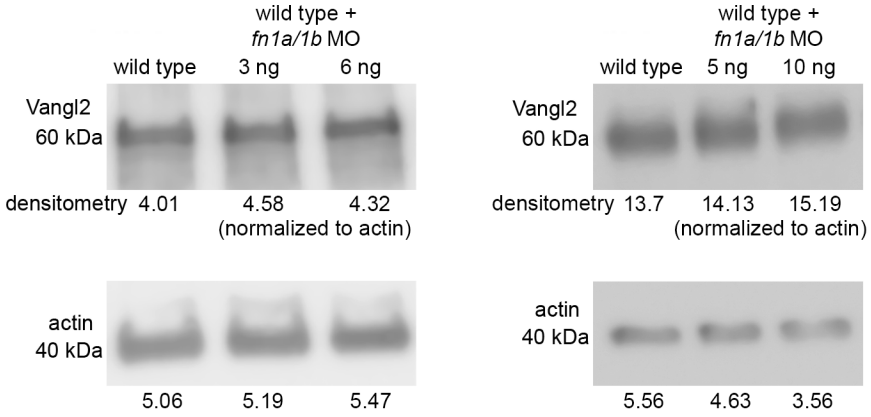

Fig. S10. Knockdown of fibronectin in *vangl2* mutant embryos. (A) Time-lapse confocal image of late gastrula stage cell expressing memGFP. *vangl2* mutant embryo injected with *fn1a/1b* morpholinos (MO). (B,C) Quantitation of the total numbers of membrane protrusions formed by *vangl2* mutant embryos injected with *fn1a/1b* MO (n=5 cells, 3 embryos). The data from wild type (WT), *vangl2* mutant embryos, and wild-type embryos injected with *fn1a/1b* MO are shown for comparison. (D) Quantitation of the total percentage of polarized large protrusions. Average values are shown ± standard deviation. ****P<0.0001; P values are versus wild type; one-way ANOVA significance test followed by Tukey HSD post-hoc tests. Scale bar, 5 μm.

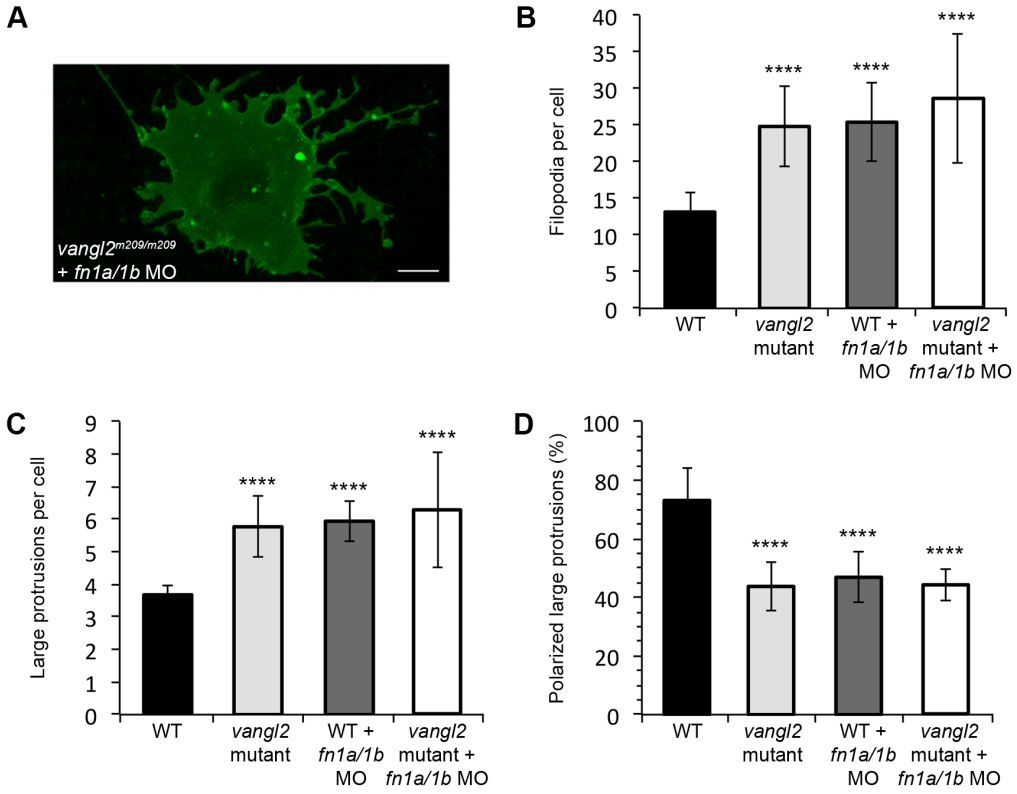

Fig. S11. *vangl2* mRNA overexpression in *fn1a/1b* morphant wild-type embryos. (A) Time-lapse confocal image of late gastrula cell expressing memGFP. *fn1a/1b* morpholino (MO) injected wild-type embryo co-injected with synthetic *vangl2* mRNA. (B,C) Quantitation of the total numbers of membrane protrusions formed by wild-type embryos injected with *fn1a/1b* MO and *vangl2* mRNA (n=5 cells, 4 embryos). The data from wild type (WT), *vangl2* mRNA injected wild-type embryos, and *fn1a/1b* MO injected wild-type embryos are shown for comparison. (D) Quantitation of the total percentage of polarized large protrusions. Average values are shown ± standard deviation. ***P*<0.01, ****P*<0.001, *****P*<0.0001; *P* values are versus wild type; one-way ANOVA significance test followed by Tukey HSD post-hoc tests. Scale bar, 5 µm.

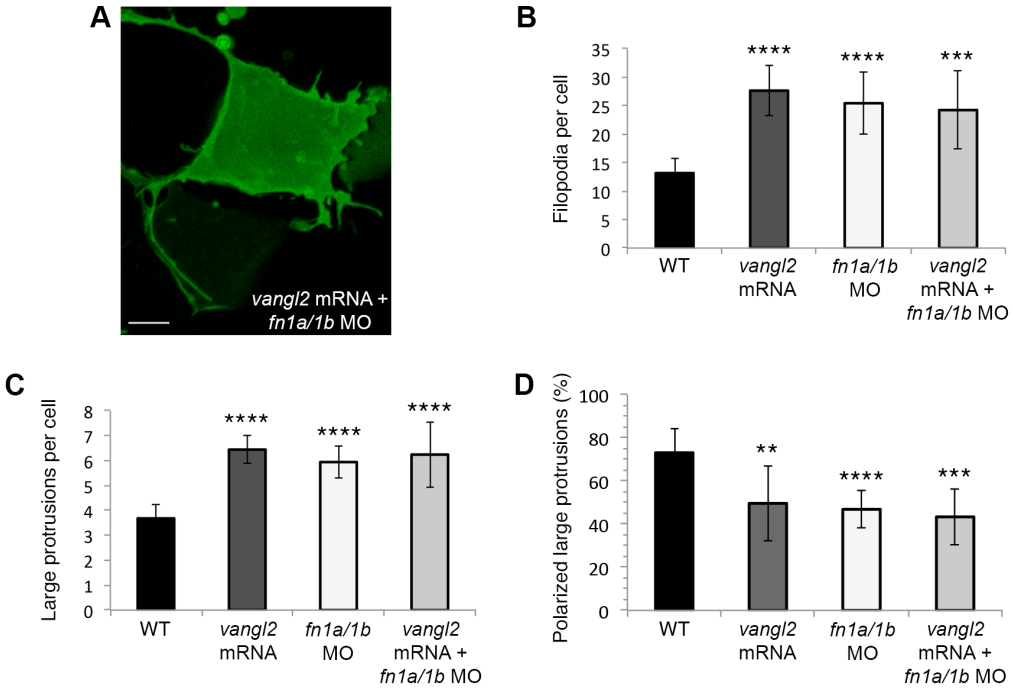

Fig. S12. Injection of *fn1a/1b* mRNA fails to rescue the *vangl2* mutant embryo convergence and extension phenotype. (A) Lateral view of a wild-type embryo at the yolk-plug closure (YPC)-tailbud stage. Black lines denote the polster-tailbud angle. (B) Lateral views of three *vangl2*$^{m209/m209}$ embryos highlighting subtle variations in the mutant convergence and extension phenotype. (C) Lateral views of three *vangl2*$^{m209/m209}$ embryos injected with *fn1a/1b* mRNA (n=50 mRNA injected homozygous mutant embryos analyzed).

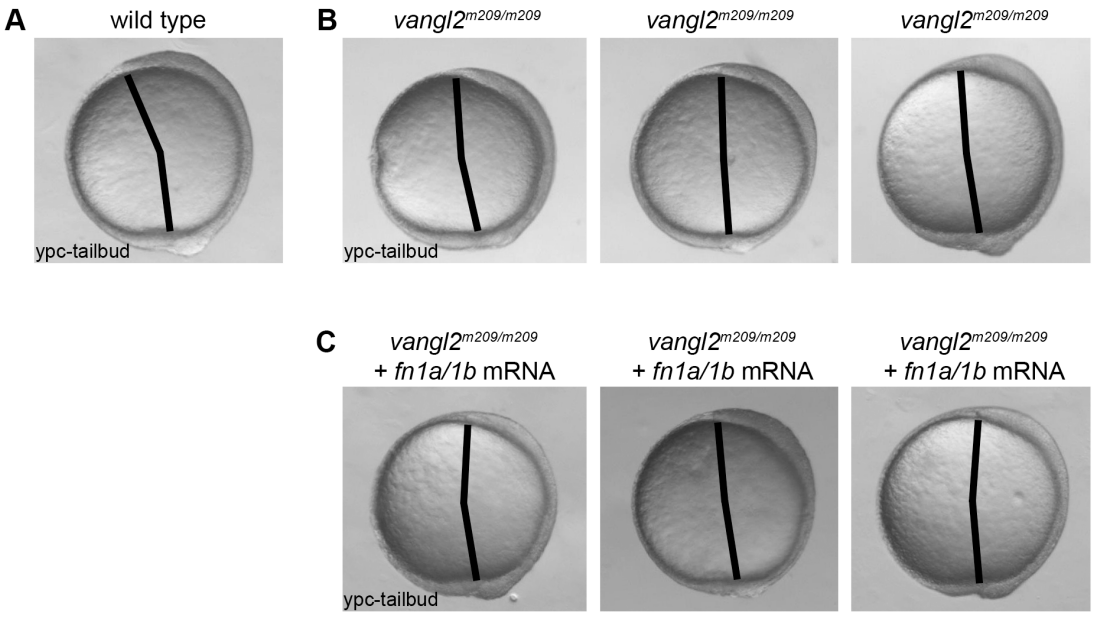

Table S1. Accumulated and Euclidean ectodermal cell translocation distances.

	Accumulated distance (μm)	Euclidean distance (μm)
wild type	19.49 +/- 8.82	18.81 +/- 8.78
vangl2$^{m209/m209}$	17.68 +/- 9.70	15.76 +/- 10.54
glypican4$^{m119/m119}$	21.22 +/- 5.05	20.02 +/- 5.18
wild type + *vangl2* mRNA	14.36 +/- 7.75	11.45 +/- 9.06
wild type + *prickle1a* morpholino	17.74 +/- 6.18	15.68 +/- 8.04
wild type + *fn1a/1b* morpholino	24.78 +/- 11.49	22.88 +/- 11.26
vangl2$^{m209/m209}$ + *fn1a/1b* mRNA	23.45 +/- 6.34	22.03 +/- 6.15

Fig. S1. Rose diagrams showing large membrane protrusion directionality around the cell circumference. Diagrams depicting the circular frequency and distribution of ectodermal cell large protrusions are shown for each experimental condition: wild type, *vangl2*$^{m209/m209}$ mutant embryos, *glypican4*$^{m119/m119}$ mutant embryos, *vangl2* mRNA injected wild-type embryos, *prickle1a* morpholino (MO) injected wild-type embryos, *fn1a/1b* MO injected embryos, and *fn1a/1b* mRNA injected *vangl2*$^{m209/m209}$ mutant embryos. The horizontal plane represents 0° and a mediolateral protrusion orientation while the vertical plane represents 90° and a anterior-posterior protrusion orientation. The position of the dorsal embryonic axis is indicated.

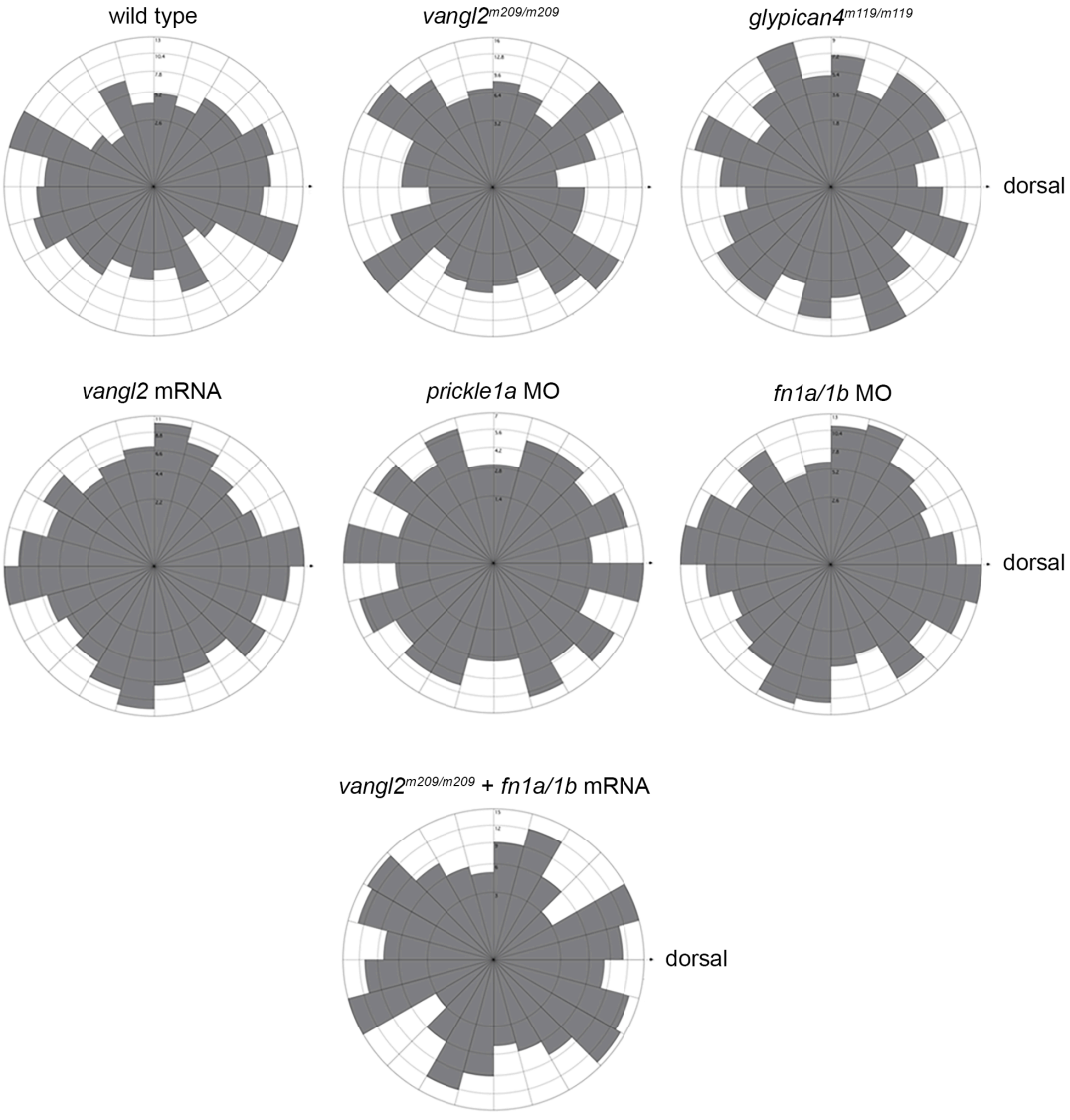

Fig. S2. Zebrafish Vangl2 polyclonal antibody validation and Vangl2 overexpression. (A) Immunofluorescence labeling of endogenous Vangl2 protein expression in wild-type (WT) tailbud stage embryo (right panel, nuclei labeled with DAPI). (B) Vangl2 expression in a wild-type embryo injected with 200 pg synthetic *vangl2* mRNA (right panel, nuclei labeled with DAPI). (C) Endogenous Vangl2 expression in a tailbud stage *vangl2*$^{vu7/vu7}$ mutant embryo. Only background fluorescence from the secondary antibody is visible. Scale bars: 5 μm in panels A and B; 20 μm panel C.

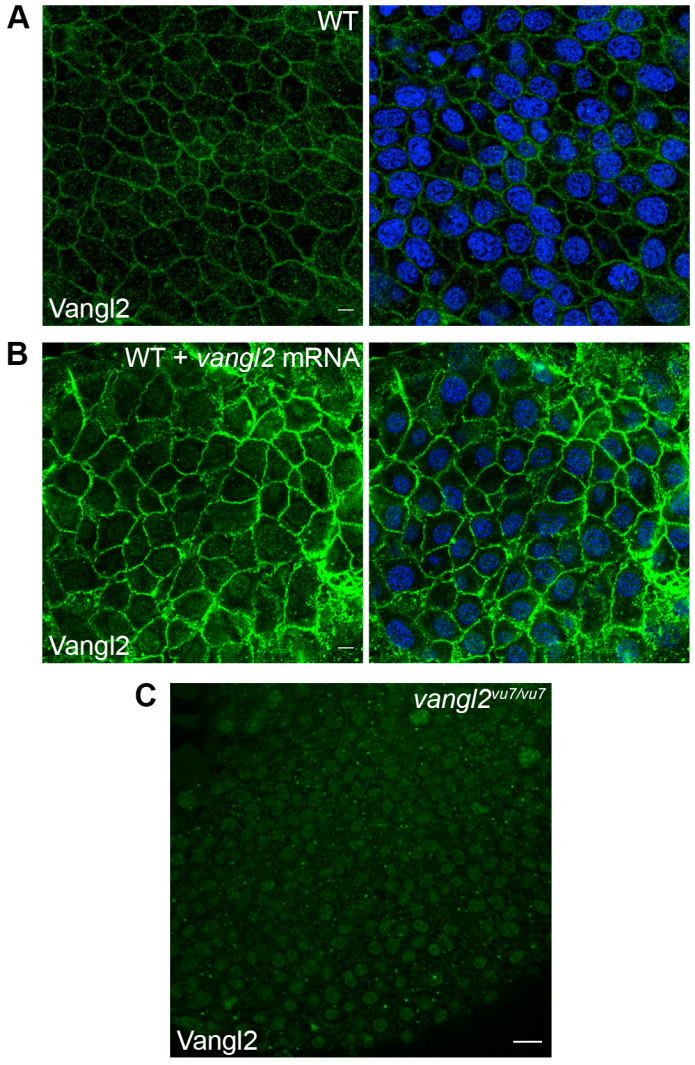

Fig. S3. Vangl2 overexpression disrupts PCP and membrane protrusion dynamics. (A) Western blot of Vangl2 protein expression in *vangl2* mRNA-injected wild-type (WT) embryos. Raw unmodified densitometry values are shown. (B) Upper panels, live images of late yolk-plug closure/tailbud stage embryos. Black lines denote the polster-tailbud angle. Lower panels, whole-mount *in situ* hybridizations performed using antisense RNA probes labeling the neural/non-neural ectoderm boundary (*dlx3b*), midline (*shha*), and prechordal mesendoderm (*ctslb*). (C) PCP and migration velocity quantitation in the ectoderm. LWR and MLA values were obtained from: wild type n values are as in Fig. 2; *vangl2*-injected wild type n=50 cells, 9 embryos. (D) Representative ectodermal cell expressing memGFP over three time points from time-lapse data. (E,F) Quantitation of the average total number of protrusions and the total percentage of polarized protrusions in wild type (n values are as in Figs 2 and 3) and *vangl2*-injected wild-type embryos (n=10 cells, 7 embryos). (G) Directed migration values (wild type n values are as in Fig. 3; *vangl2*-injected n=43 cells, 9 embryos). (H) Schematic representations of the migration paths of individual ectodermal cells. Origins (arrows) standardized for comparison. Dorsal is to the right. Average values are shown ± standard deviation. $^{**}P<0.01$, $^{****}P<0.0001$; *P* values are versus wild type; two-tailed unpaired *t*-test. Scale bar, 5 μm.

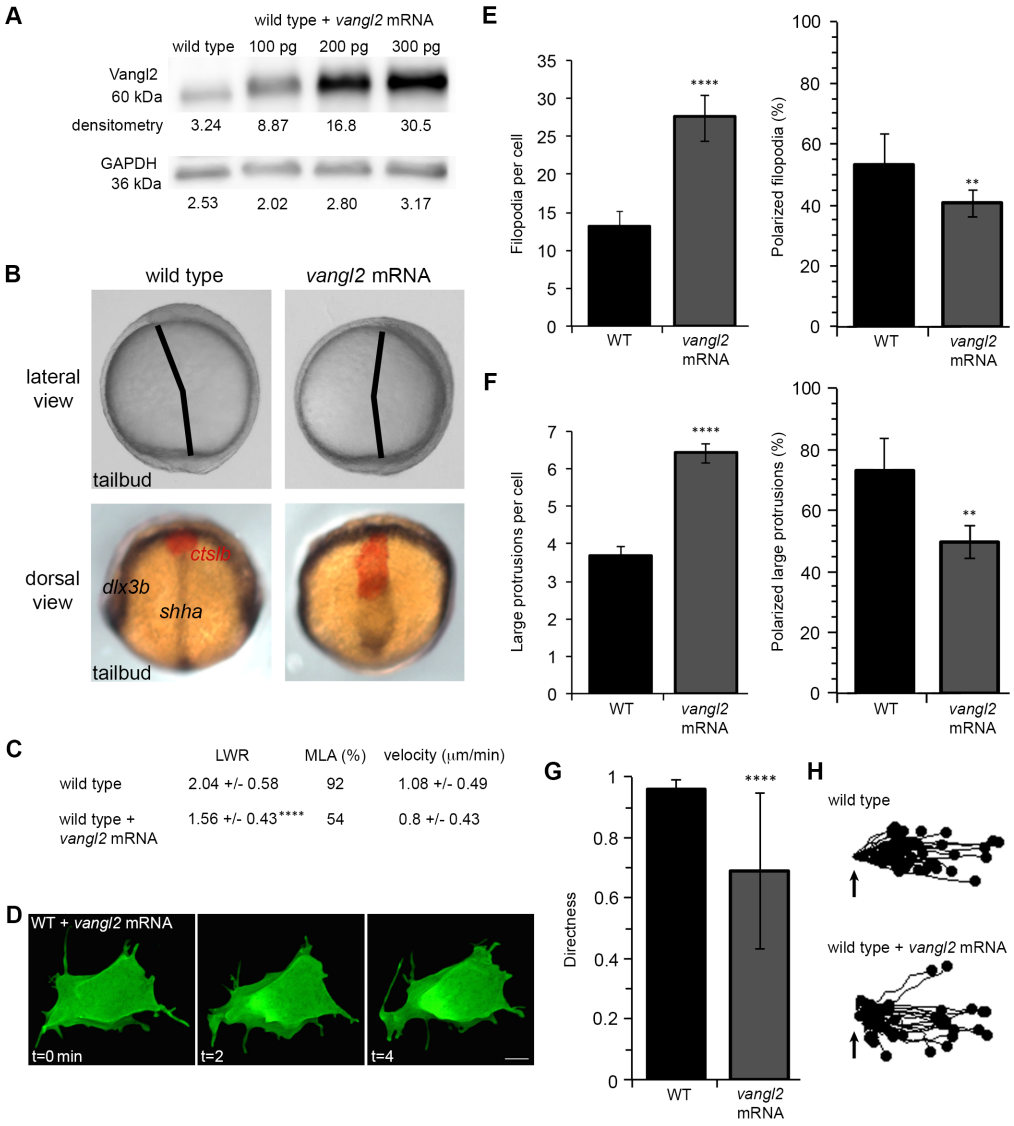

Figure S3

Fig. S4. Vangl2 expression in polarized migrating gastrula cells. (A) Tailbud-1-somite stage wild-type lateral ectodermal cells injected with memRFP and GFP-VANGL2 synthetic mRNA. (B,D) Plot profiles of fluorescence intensity (F.I.) across the anterior/posterior (B) and leading edge/trailing edge (D) axes of single ectodermal cells. (C,E) memRFP and GFP-VANGL2 anterior/posterior (C) and leading edge/trailing edge (E) membrane F.I. ratios for individual lateral ectodermal cells (anterior/posterior n=18 cells, 15 embryos; leading edge/trailing edge n=20 cells, 15 embryos). Horizontal and vertical red and green lines indicate averages. n.s. not significant; two-tailed paired *t*-test. Scale bars, 5 μm.

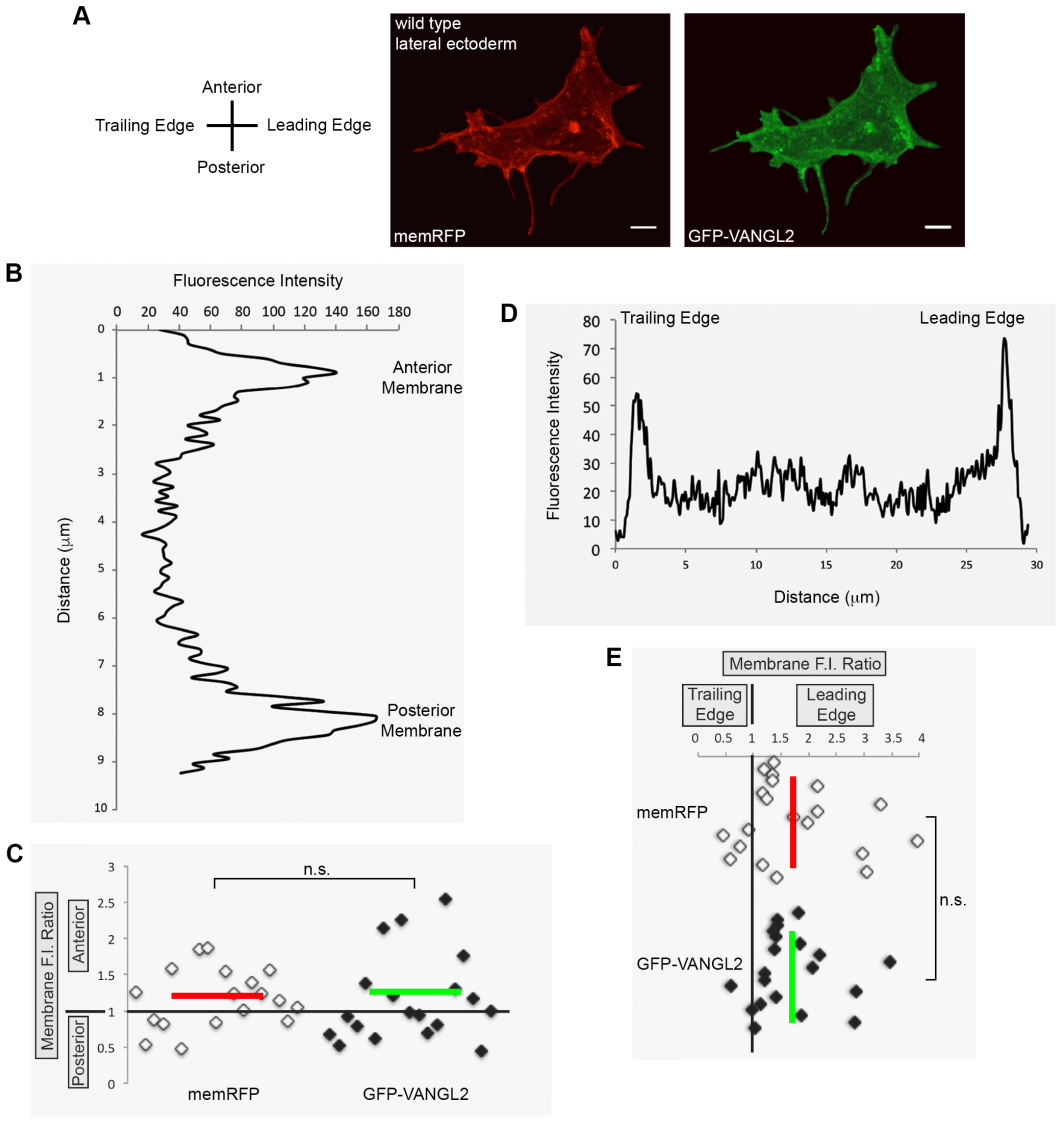

Fig. S5. GFP-VANGL2 localization in protrusive and non-protrusive membrane domains. (A) Lateral ectodermal cell labeled with memRFP and GFP-VANGL2. Arrows denote a forming non-polarized large protrusion. Arrowheads show a non-protrusive membrane domain. memRFP and GFP-VANGL2 fluorescence intensity (F.I.) ratios for (B) protrusive/non-protrusive membrane domains (n=9 protrusions, 6 embryos) and (C) polarized/non-polarized large protrusions (n=14 protrusions, 5 embryos). Vertical red and green lines indicate the averages. *P<0.05, n.s. not significant; two-tailed paired t-test. Scale bars, 5 μm.

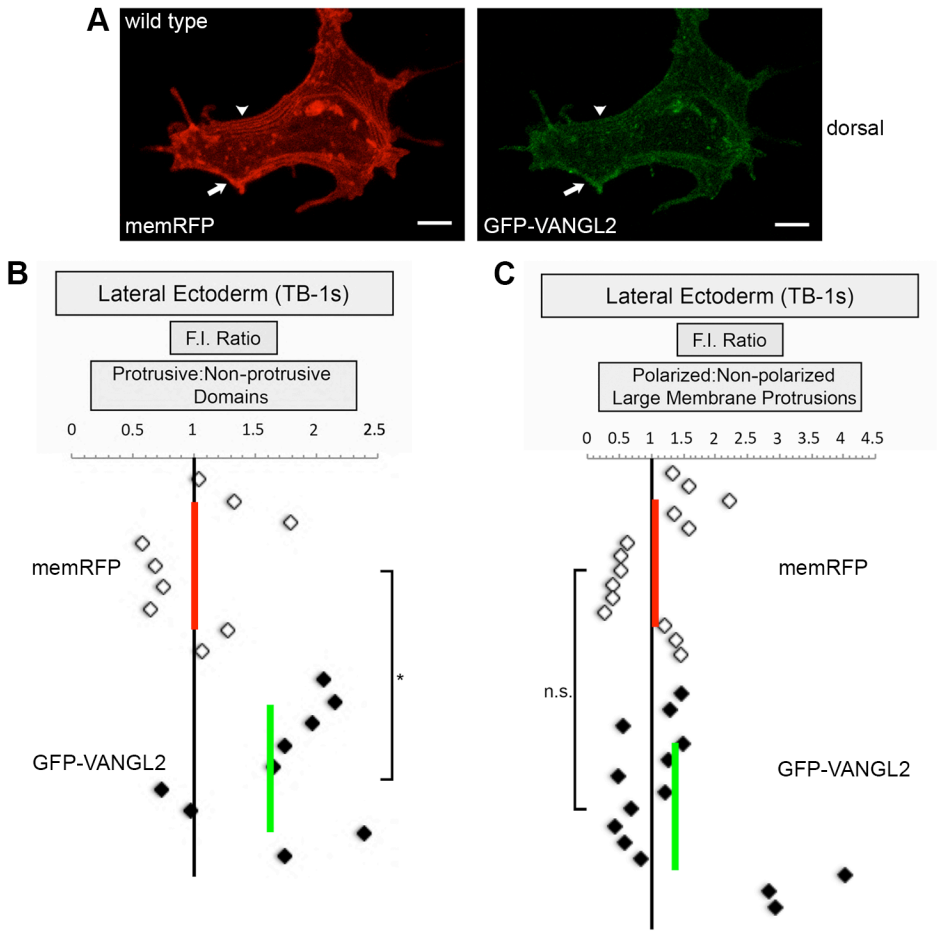

Fig. S6. Morpholino knockdown disrupts fibronectin expression and fibrillogenesis. (A) Immunofluorescence labeling of fibronectin expression in tailbud stage wild-type embryo and wild-type embryos injected with either 5 ng or 10 ng of each *fibronectin* morpholino (MO). (B) Injection of *fn1a/1b* synthetic mRNA rescues the *fn1a/1b* morpholino ECM phenotype. Bottom images in (A) and (B) show DAPI-labeled nuclei. Scale bars, 5 µm.

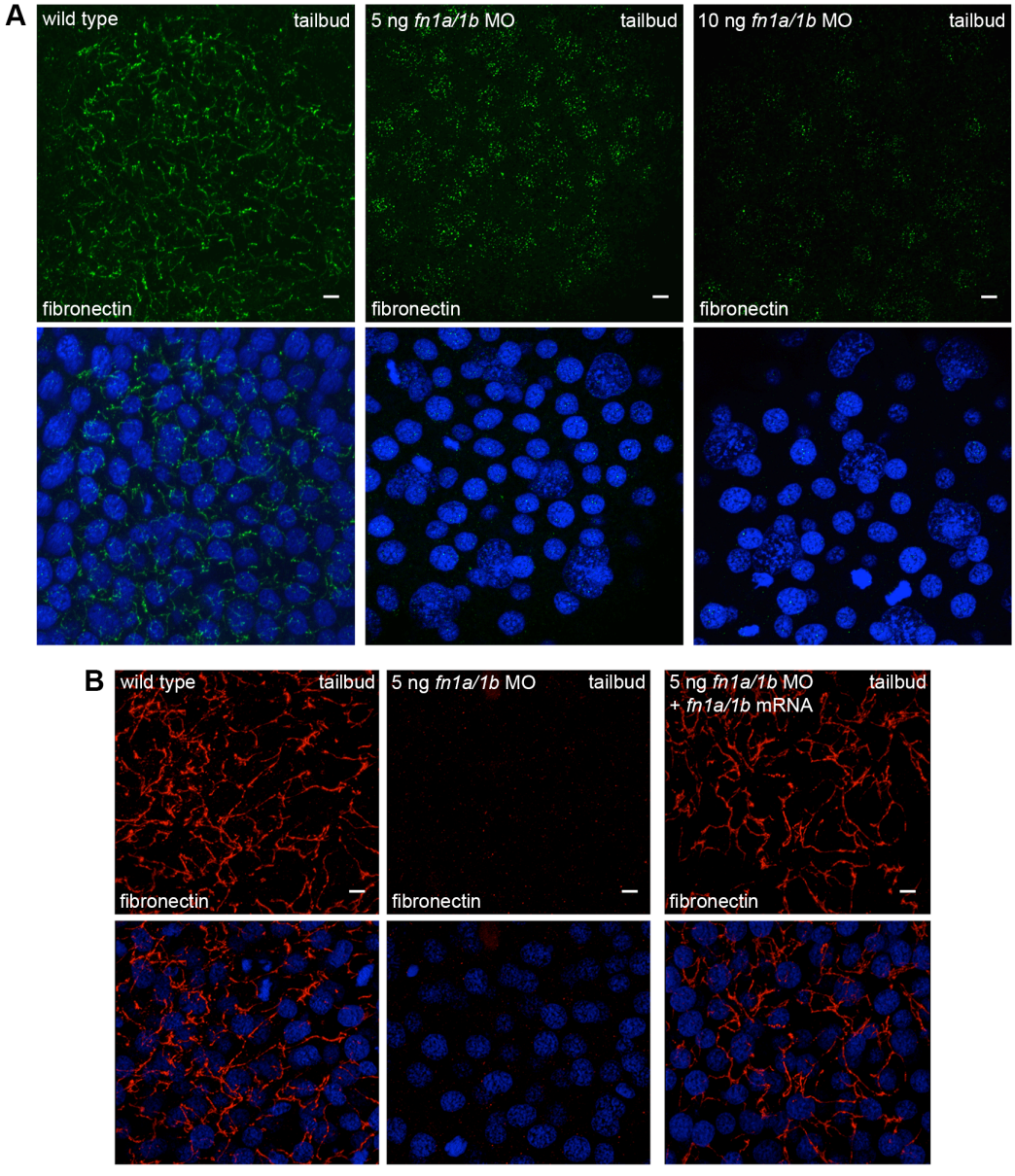

Fig. S7. Wild type and *vangl2* morphant membrane protrusive activity at mid-gastrulation. (A) Time-lapse confocal images of 80% epiboly epiblast cells expressing memGFP. WT, wild type. (B,C) Quantitation of the total numbers of membrane protrusions formed by wild type (n=9 cells, 7 embryos) and wild-type embryos injected with *vangl2* morpholino (MO) (n=10 cells, 6 embryos). (D) Quantitation of the total percentage of polarized large protrusions. Average values are shown ± standard deviation. ***P*<0.01; *P* values are versus wild type; two-tailed unpaired *t*-test. Scale bars, 5 µm.

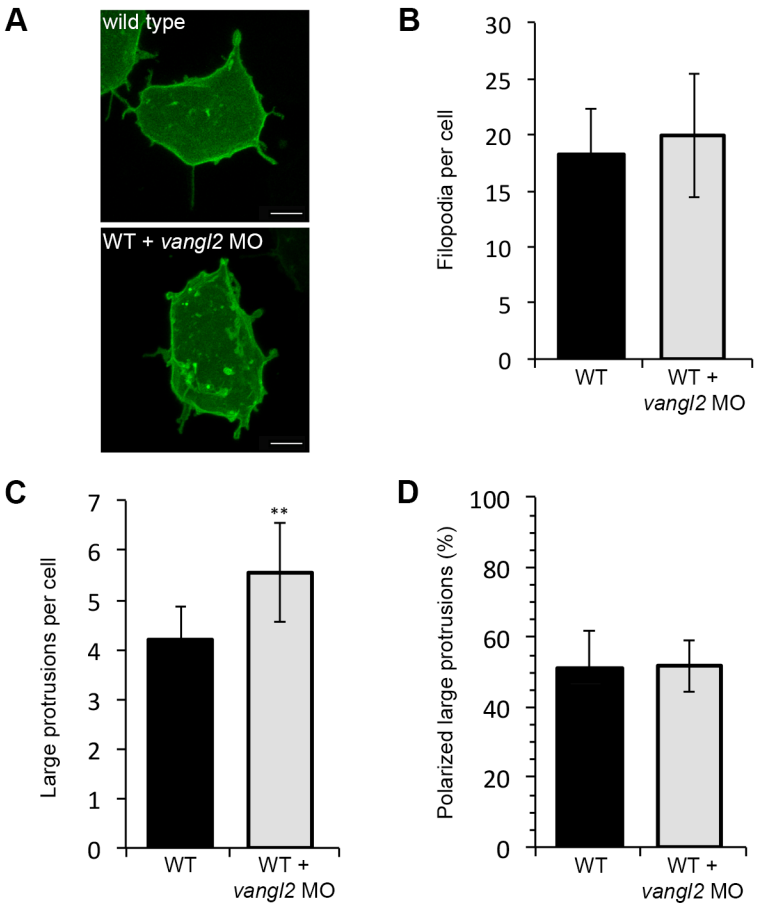

Fig. S8. Fibronectin is not required for Vangl2 expression at 60% epiboly. (A) Immunofluorescence labeling of Vangl2 protein expression in wild type and *fn1a/1b* morpholino (MO)-injected wild-type embryos without (left panels) and with (right panels) DAPI nuclear labeling. (B) Representative plot profiles showing the average fluorescence intensities across single epiblast cells in wild type (n=30 cells, 3 embryos) and *fn1a/1b* morphant embryos (n=30 cells, 3 embryos). Scale bars, 5 μm.

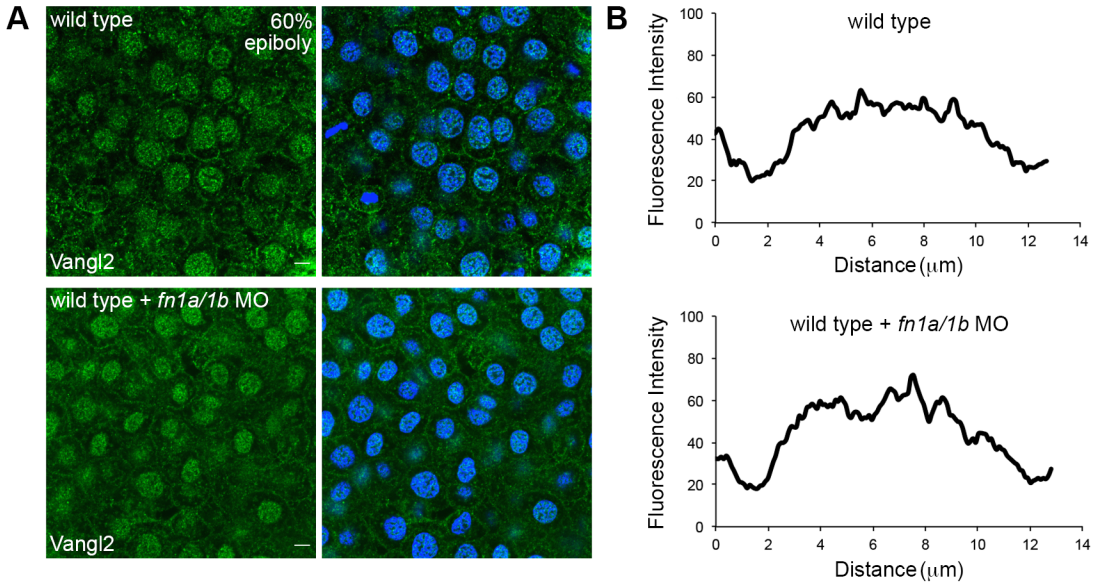

Fig. S9. Western blot analysis of Vangl2 expression in *fibronectin* morphants. Blots of total protein extracts from wild-type control embryos and wild-type embryos injected with 3, 6, 5, and 10 ng of each *fibronectin* morpholino (MO). Vangl2 labeled with a rabbit polyclonal antibody and actin loading control. Densitometry numbers for Vangl2 are normalized to actin.

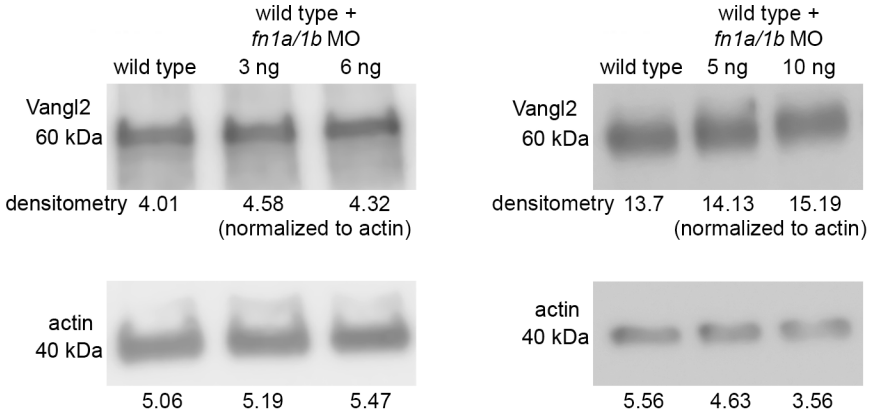

Fig. S10. Knockdown of fibronectin in *vangl2* mutant embryos. (A) Time-lapse confocal image of late gastrula stage cell expressing memGFP. *vangl2* mutant embryo injected with *fn1a/1b* morpholinos (MO). (B,C) Quantitation of the total numbers of membrane protrusions formed by *vangl2* mutant embryos injected with *fn1a/1b* MO (n=5 cells, 3 embryos). The data from wild type (WT), *vangl2* mutant embryos, and wild-type embryos injected with *fn1a/1b* MO are shown for comparison. (D) Quantitation of the total percentage of polarized large protrusions. Average values are shown ± standard deviation. ****P<0.0001; P values are versus wild type; one-way ANOVA significance test followed by Tukey HSD post-hoc tests. Scale bar, 5 μm.

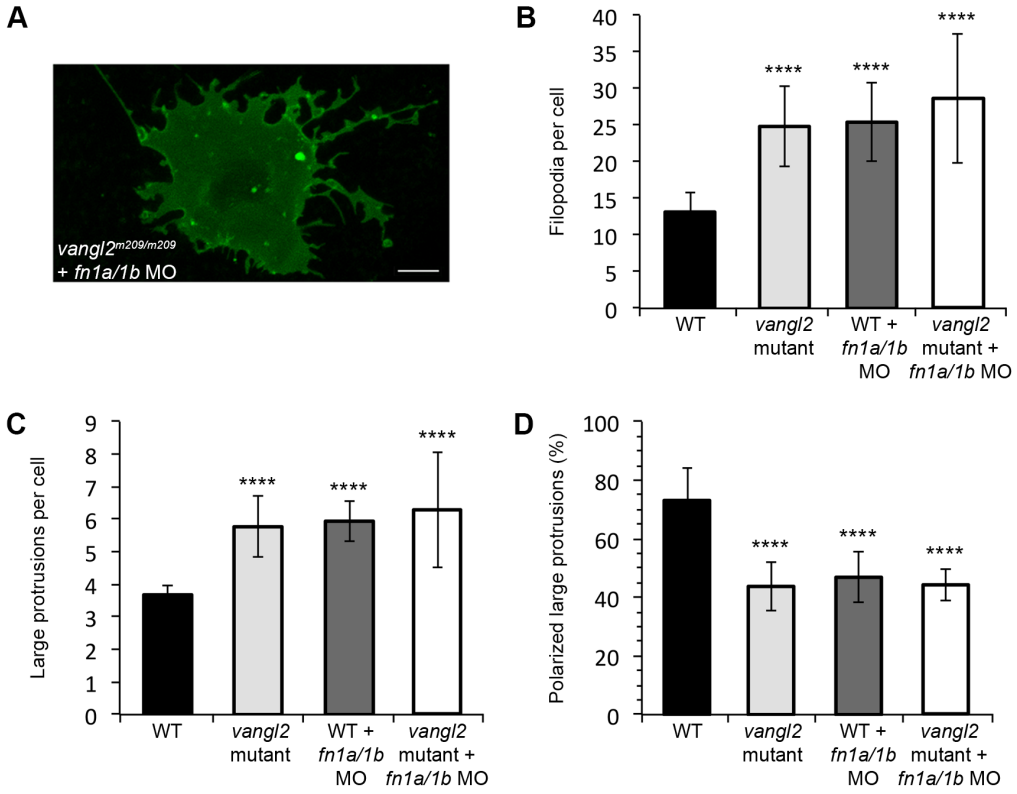

Fig. S11. *vangl2* mRNA overexpression in *fn1a/1b* morphant wild-type embryos. (A) Time-lapse confocal image of late gastrula cell expressing memGFP. *fn1a/1b* morpholino (MO) injected wild-type embryo co-injected with synthetic *vangl2* mRNA. (B,C) Quantitation of the total numbers of membrane protrusions formed by wild-type embryos injected with *fn1a/1b* MO and *vangl2* mRNA (n=5 cells, 4 embryos). The data from wild type (WT), *vangl2* mRNA injected wild-type embryos, and *fn1a/1b* MO injected wild-type embryos are shown for comparison. (D) Quantitation of the total percentage of polarized large protrusions. Average values are shown ± standard deviation. ***P*<0.01, ****P*<0.001, *****P*<0.0001; *P* values are versus wild type; one-way ANOVA significance test followed by Tukey HSD post-hoc tests. Scale bar, 5 µm.

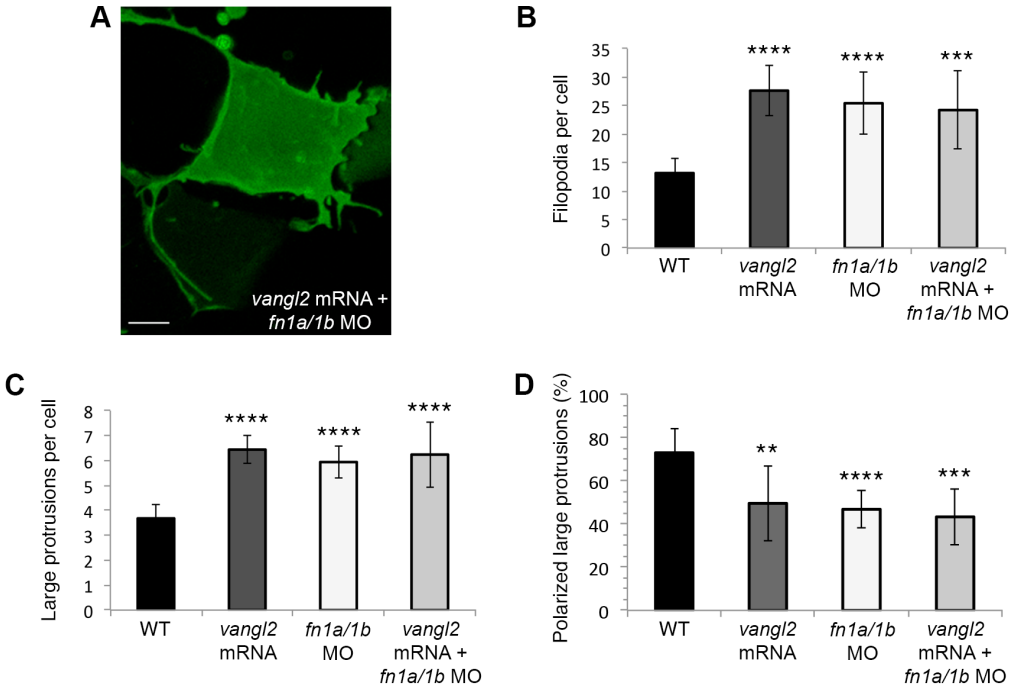

Fig. S12. Injection of *fn1a/1b* mRNA fails to rescue the *vangl2* mutant embryo convergence and extension phenotype. (A) Lateral view of a wild-type embryo at the yolk-plug closure (YPC)-tailbud stage. Black lines denote the polster-tailbud angle. (B) Lateral views of three *vangl2*$^{m209/m209}$ embryos highlighting subtle variations in the mutant convergence and extension phenotype. (C) Lateral views of three *vangl2*$^{m209/m209}$ embryos injected with *fn1a/1b* mRNA (n=50 mRNA injected homozygous mutant embryos analyzed).

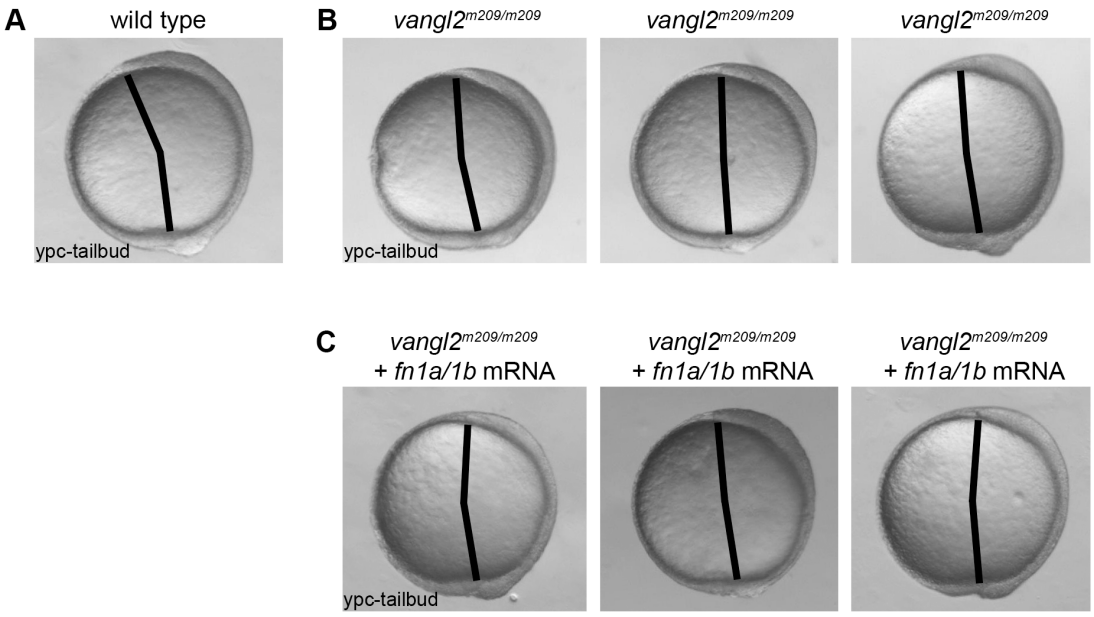

Table S1. Accumulated and Euclidean ectodermal cell translocation distances.

	Accumulated distance (μm)	Euclidean distance (μm)
wild type	19.49 +/- 8.82	18.81 +/- 8.78
vangl2$^{m209/m209}$	17.68 +/- 9.70	15.76 +/- 10.54
glypican4$^{m119/m119}$	21.22 +/- 5.05	20.02 +/- 5.18
wild type + *vangl2* mRNA	14.36 +/- 7.75	11.45 +/- 9.06
wild type + *prickle1a* morpholino	17.74 +/- 6.18	15.68 +/- 8.04
wild type + *fn1a/1b* morpholino	24.78 +/- 11.49	22.88 +/- 11.26
vangl2$^{m209/m209}$ + *fn1a/1b* mRNA	23.45 +/- 6.34	22.03 +/- 6.15